

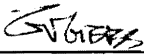
HIGH TEMPERATURE CRYSTAL CHEMISTRY OF HYDROUS  
Mg- AND Fe-RICH CORDIERITES

by


Michael F. Hochella, Jr.


Thesis submitted to the Graduate Faculty of the  
Virginia Polytechnic Institute and State University  
in partial fulfillment of the requirements for the degree of  
MASTER OF SCIENCE  
in  
Geological Sciences

APPROVED:

  
\_\_\_\_\_  
G.V. Gibbs, Chairman

  
\_\_\_\_\_  
P.H. Ribbe

  
\_\_\_\_\_  
F.K. Ross

  
\_\_\_\_\_  
F.D. Bloss

July, 1977

Blacksburg, Virginia

LD  
S655  
V855  
1977  
H62  
c. 2

## ACKNOWLEDGMENTS

I wish to thank Dr. G.V. Gibbs as chief advisor and friend. I wish to thank Dr. F.D. Bloss, Dr. P.H. Ribbe, and especially Dr. F.K. Ross in their roles as thesis advisors. Thanks also go to Dr. G.E. Brown of Stanford University for a week of instruction in high temperature experimental techniques and for the collection of the x-ray data for the White Well cordierite at high temperatures; Dr. E.P. Meagher of the University of British Columbia for running the *DLS* calculations; Charles W. Huggins of the U.S. Bureau of Mines for the thermogravimetric analysis of the White Well cordierite; Ramonda Haycocks for the typing of the manuscript; and Sharon Chiang and Robert Boyd for the drafting of the figures. This study was supported by the Earth Sciences Section of the National Science Foundation through grant DES75-14912.

## TABLE OF CONTENTS

	Page
Acknowledgments . . . . .	ii
List of Tables. . . . .	v
List of Figures . . . . .	vi
Introduction. . . . .	1
Experimental Detail and Observations. . . . .	4
<i>Specimens.</i> . . . .	4
<i>Data Collection and Refinements.</i> . . . .	6
<i>Isotropic Temperature Factors.</i> . . . .	10
<i>Cell Parameters.</i> . . . .	13
Structure . . . . .	18
Discussion. . . . .	21
<i>Tetrahedral and Octahedral Bond Length Expansion</i> . . .	21
<i>A Structural Interpretation of the Thermal Expansion of Cordierite.</i> . . . .	23
<i>Orientation of the Water Molecules in the White Well Cordierite.</i> . . . .	30
<i>The Effects of Heating on Channel Constituents</i> . . . .	32
<i>The State of the White Well Cordierite after Heating.</i> . . . .	34
References. . . . .	40
Appendix A: The Pseudo-Axes of Cordierite. . . . .	45
Appendix B: Installation, Calibration, and Operating Procedures for a Single-Crystal Heater in Conjunction with a Four-Circle Diffractometer . . . . .	51
Appendix C: Observed (Fo) and Calculated (Fc) Structural Amplitudes for the White Well and Dolni Bory Cordierites at Various Temps. . .	73

TABLE OF CONTENTS, continued

	Page
Appendix D: Final Fractional Coordinates and Thermal Parameters for the White Well and Dolni Bory Cordierites. . . . .	87
Appendix E: Interatomic Distances and Angles for the White Well and Dolni Bory Cordierites at Various Temps . . . . .	97
Vita. . . . .	110
Abstract. . . . .	

LIST OF TABLES

Table	Page	
1	Cell parameters (24°C), distortion index ( $\Delta$ ), density ( $\rho$ ), and composition of the White Well and Dolni Bory cordierites . . . . .	5
2	Results of the anisotropic refinements for the White Well and Dolni Bory cordierites . . . . .	8
3	Cell edges ( $\text{\AA}$ ), cell volume ( $\text{\AA}^3$ ), and calculated distortion index <i>vs</i> temperature for White Well cordierite . . . . .	14
4	Polyhedral volumes ( $\text{\AA}^3$ ) <i>vs</i> temperature for White Well cordierite . . . . .	22

## LIST OF FIGURES

Figure		Page
1	Isotropic equivalent temperature factors for the White Well cordierite plotted as a function of temperature . . . . .	11
2	Isotropic equivalent temperature factors for the Dolni Bory cordierite plotted as a function of temperature . . . . .	12
3	Axial expansion <i>vs</i> temperature for two synthetic indialites and the White Well cordierite. . . . .	16
4	ORTEP drawing of the cordierite structure viewed down <i>c</i> . . . . .	19
5	An ORTEP stereopair drawing showing the four-membered rings which are linked into chains paralleling <i>c</i> . . . . .	20
6	The <i>a</i> and <i>b</i> cell edges <i>vs</i> the octahedral volume for both the White Well and Dolni Bory cordierites at various temperatures. . . . .	24
7	The <i>a</i> and <i>b</i> cell edges <i>vs</i> the thickness of the M-octahedron measured along <i>a</i> , $t_a$ , and along <i>b</i> , $t_b$ , for the White Well and Dolni Bory cordierites at various temperatures. . . . .	25
8	Rotation of the six-membered rings in the White Well cordierite . . . . .	27
9	Stereographic projection of the actual displacements of the independent tetrahedral ring cations from 24°C to 775°C in the White Well cordierite. . . . .	28
10	The length of the <i>c</i> -cell edge <i>vs</i> one T-O-M and two O-T-O angles at various temperatures for the White Well cordierite. . . . .	29
11	X-ray $\Delta\rho$ map (24°C) showing the elongated oxygen peak along the <i>x</i> axis. . . . .	31

LIST OF FIGURES, continued

Figure		Page
12	Neutron $\Delta\rho$ map (24°C) showing the negative scattering of the hydrogens in the 100 plane at $x = .01$ . . . . .	33
13a	X-ray $\Delta\rho$ map of the White Well cordierite showing the peaks ascribed to the channel constituents at 24°C . . . . .	35
13b	X-ray $\Delta\rho$ map of the White Well cordierite showing the peaks ascribed to the channel constituents at 375°C. . . . .	36
13c	X-ray $\Delta\rho$ map of the White Well cordierite showing the peaks ascribed to the channel constituents at 775°C. . . . .	37
13d	X-ray $\Delta\rho$ map of the White Well cordierite showing the peaks ascribed to the channel constituents at 24°C (after heating) . . . . .	38



## INTRODUCTION

The expansion properties of the mineral cordierite,  $(\text{Mg,Fe})_2\text{Al}_4\text{Si}_5\text{O}_{18}\cdot n\text{H}_2\text{O}$ , have attracted the interests of ceramists because of its value as a thermal shock resistant material. It has also attracted the interests of mineralogists and petrologists because of its polymorphism and widespread occurrence in metamorphic terraines. The polymorphism of cordierite may not be as simple as once believed but may involve a two-step ordering process like that evinced by the alkali feldspars (Meagher and Gibbs, 1967). Apparently it can exist in all intermediate structural states between an hexagonal polymorph called indialite (Miyashiro and Iiyama, 1954; Meagher and Gibbs, 1977) and an orthorhombic form called low cordierite (Miyashiro *et al.*, 1955; Schreyer and Schairer, 1961; Gibbs, 1966; Meagher and Gibbs, 1966; Meagher, 1967; Cohen *et al.*, 1977). In low cordierite the Al and Si atoms are ordered in a tetrahedral framework of  $\text{Al}_4\text{Si}_5\text{O}_{18}$  composition (Cohen *et al.*, 1977) whereas in indialite they are only partly ordered (Meagher and Gibbs, 1977). The existence of a completely disordered polymorph of cordierite has yet to be substantiated.

According to Newton (1973), cordierite plays a poorly understood yet important role in regionally metamorphosed rocks of the amphibolite and granulite facies. It is also a common constituent of thermally metamorphosed rocks, particularly those lacking well-developed foliation and derived from argillaceous sediments. In addition, it is frequently associated with anthophyllite or gedrite

in massive metamorphosed sulfide deposits and occurs in granitic pegmatites with quartz as micropegmatitic intergrowths. The Fe-Mg distribution for coexisting cordierite and garnet pairs has been measured experimentally by Hensen and Green (1971) and Currie (1971) and found to be potentially valuable to petrologists as a geobarometer-geothermometer.

Because of its unusually low thermal expansion, Mg-rich cordierite is an extremely important and valuable mineral in the ceramic industry. It is used as an insulator for spark plugs (Fessler, 1938), as a refractory coating on metals for internal combustion engines (Desmarquest, 1965), in the production of dolomitic types of refractories (Nagasaki *et al.*, 1970) and low expansion concrete (Magnan, 1971), and as a catalytic support for the treatment of waste gas (Soejima, 1974) and automobile exhaust emissions (Lachman and Lewis, 1973; Takao *et al.*, 1974). Perhaps its most important application in the future will be in the fabrication of turbine engines (Gostlow and Restall, 1972). Fe-rich cordierite has been produced in industry but only as a by-product in blast-furnace linings (Richardson, 1949), in "black cores" in stoneware pipes (Lach, 1974), and even in building-brick (Rathgeber and Fowler, 1966). Ceramists are not particularly interested in Fe-rich cordierite because it is much more difficult to synthesize and because it shows moderate oxidation at high temperatures.

In light of the increasing interest in this mineral, this study was undertaken to determine (1) the effect of heating upon the Al/Si

distribution in the tetrahedral framework, (2) the crystal structure of hydrous Mg- and Fe-rich low cordierite as a function of temperature in an attempt to clarify the unusual thermal expansion properties of the mineral, (3) the orientation of the water molecules in the channels of the structure, and (4) the effects of heating on water and the alkali atoms in these channels.

## EXPERIMENTAL DETAIL AND OBSERVATIONS

### *Specimens*

The Mg-rich cordierite used in our study, designated the White Well cordierite, was previously described and used in a combined X-ray and neutron diffraction study by Cohen *et al.* (1977). It is one of the most Mg-rich specimens ever to be reported in nature (see Table 1). We assumed that our crystal ( $0.30 \times 0.22 \times 0.22$  mm) and those used by Cohen *et al.* (1977) had identical chemical compositions and crystal structures because they had statistically identical cell dimensions and were selected from the same specimen (approximately a 4 mm cube). The room temperature data (before heating) listed in Appendices D and E were taken from Cohen *et al.* (1977).

The Fe-rich cordierite used in our study (Table 1), designated the Dolni Bory cordierite, was collected from a pegmatite near Dolni Bory, Western Moravia, Czechoslovakia (Stanek and Miskovsky, 1964). Many of its single crystals were sector twinned; however, two exhibiting sharp and uniform extinction were found suitable for structure determination. Both crystals measured approximately 0.25 mm on a side. After orientation (see Appendix A) using the optical spindle stage techniques of Bloss (1977), crystals of the White Well and Dolni Bory cordierites were sealed in evacuated quartz capillaries to inhibit the oxidation of the iron. Each was then allowed to equilibrate for at least 12 hours at the temperature of the measurement before data collection was begun. The temperature fluctuations for the heater during the measurement were not more than  $\pm 10^\circ$  at  $375^\circ\text{C}$  and  $\pm 15^\circ$  at

TABLE 1

Cell parameters (24°C), distortion index ( $\Delta$ ), density ( $\rho$ ) and composition of the White Well and Dolni Bory cordierites

	White Well	Dolni Bory
$a$	17.088(3) Å	17.230(5) Å
$b$	9.734(2)	9.835(3)
$c$	9.359(1)	9.314(3)
$\Delta$	0.25°	0.21°
$\rho$	2.56 g/cm <sup>3</sup>	2.78 g/cm <sup>3</sup>
Formulas* (based on 18 oxygens)		
T cations	Si <sub>5.01</sub> Al <sub>3.95</sub>	Si <sub>4.91</sub> Al <sub>4.05</sub>
M cations	Mn <sub>0.01</sub> Mg <sub>1.91</sub> Fe <sub>0.08</sub> <sup>2+</sup>	Mn <sub>0.08</sub> Mg <sub>0.25</sub> Fe <sub>1.65</sub> <sup>2+</sup>
Alkalis	Na <sub>0.05</sub> K <sub>0.02</sub> Ca <sub>0.02</sub>	Na <sub>0.15</sub> Ca <sub>0.05</sub>
Water	(H <sub>2</sub> O) <sub>0.56</sub>	(H <sub>2</sub> O) <sub>0.61</sub>

\* White Well cordierite composition reported by Pryce (1973); Dolni Bory cordierite composition reported by Stanek and Miskovsky (1964).

775°C. Those interested in a detailed description of the crystal mounting techniques and the single crystal heater should consult Brown *et al.* (1973) and Appendix B of this thesis.

#### *Data Collection and Refinements*

The intensity data for the structural refinements were collected over a range of  $5^\circ$  to  $60^\circ 2\theta$ , the upper limit being imposed by the heater configuration. Three standard reflections measured every 30 reflections indicated that machine drift was within acceptable limits so no drift correction was applied. The observed intensities, corrected for Lorentz-polarization effects, were converted to  $|F(\text{obs})|$  with the program DATALIB.<sup>1</sup> Since the linear absorption coefficients for the White Well ( $9.1 \text{ cm}^{-1}$ ) and the Dolni Bory ( $25.2 \text{ cm}^{-1}$ ) cordierites were relatively small and since the crystal of the latter was lost, no absorption corrections were applied to the data sets. An approximate extinction correction was made and least-squares refinements were calculated first using isotropic and later using anisotropic temperature factor models. The  $|F(\text{obs})|$ 's were weighted in the refinements according to the procedure described by Cohen (1975). In the refinement of each structure, reflections were automatically rejected at the  $2\hat{\sigma}$  level for the White Well cordierite and at  $3\hat{\sigma}$  for the Dolni Bory cordierite. In our refinement of the White Well cordierite, we neglected the channel constituents. On the other

---

<sup>1</sup> Catalogued in the World List of Crystallography Computer Programs (3rd edition).

hand, while neglecting the water, we included the alkali atoms in our refinement for the Dolni Bory cordierite because of their greater abundance. The number of accepted reflections and the weighted and unweighted R-factors for the anisotropic refinements are given for both cordierites in Table 2. (See Appendix C for a complete listing of calculated and observed structure factors for each refinement.) The final positional parameters and anisotropic temperature factors, as well as the isotropic equivalent temperature factors for the non-equivalent atoms in the White Well and Dolni Bory cordierites, are listed in Appendix D. Selected interatomic distances and angles, calculated with the program ORFFE3,<sup>1</sup> are given in Appendix E. The bond distances and angles were not corrected for thermal motion because such corrections cannot be accurately or meaningfully made at this time.

Because the R-factors for the Dolni Bory cordierite were slightly higher than expected, an attempt was made to refine its structure within the constraints of subgroup symmetry  $C_{2c}2$  (see Appendix D). During refinement, the parameters of the pairs of pseudo-symmetrically related atoms were not varied simultaneously but were varied alternately to avoid high correlation coefficients (Fang and Robinson, 1977). The results of the final anisotropic refinement on 1203 reflections recorded at 24°C yielded an unweighted R-factor of 0.067 and a weighted R of 0.058. Even though this drop in the R-factor was significant according to the statistics of Hamilton (1965), the lower symmetry space group was not accepted because (1) the fractional positional parameters were

TABLE 2

Results of the anisotropic refinements for  
the White Well and Dolni Bory cordierites

Cordierite	Temperature	# of accepted reflections	R-factor	
			UNW	W
White Well	24°C (after Cohen <i>et al.</i> )	1057	0.033	0.041
	375°C	1077	0.041	0.066
	775°C	994	0.056	0.087
	24°C (after heating)	1176	0.038	0.061
Dolni Bory	24°C	1203	0.073	0.063
	375°C	716	0.061	0.063



statistically identical with those of the *Coom* refinement except for the M site and (2) more than half of the atoms were calculated to have nonpositive-definite temperature factors.

Precession photographs of the White Well cordierite recorded following the heating experiment showed powder rings of weak intensity identified as the diffraction pattern of hematite. Later, when the Dolni Bory cordierite was heated above 600°C, the crystal changed from colorless to amber while the peak intensities dropped off drastically obviating the collection of additional data. A second crystal was selected and the measurements were repeated but again the peak intensities dropped off markedly at temperatures above 600°C. Precession photographs recorded after the second set of measurements showed the same faint powder rings of the hematite diffraction pattern. Rathgeber and Fowler (1966) have completed open air heating experiments at 1150°C on stoichiometric Fe-cordierite in which they noticed a reddening of the crystals, a 40% decrease in measured X-ray powder diffraction peak intensity, and the formation of hematite (see also Strunz *et al.*, 1971). On the other hand, hedenbergite,  $\text{CaFeSi}_2\text{O}_6$ , was successfully heated as high as 1000°C for data collection by Cameron *et al.* (1973) using the same heater and mounting techniques employed in our study. Also Brown and Prewitt (1973) heated an olivine ( $\text{Fa}_{31}$ ) to 710°C in an evacuated capillary with no loss in the intensities of the diffraction data nor evidence of oxidation or breakdown. However, unlike cordierite, both of these minerals lack loosely bound water molecules and Fe atoms in the channels (Goldman *et al.*, 1977). Upon heating, these components apparently react even

in a thoroughly evacuated capillary to produce hematite. The decrease in the intensities of the diffraction data recorded for the Dolni Bory cordierite indicates that octahedral Fe is also involved in the reaction to form hematite which results in partial disruption of the Fe-cordierite structure.

#### *Isotropic Temperature Factors*

Isotropic equivalents of the anisotropic temperature factors for the White Well and Dolni Bory cordierites were calculated and are listed in Appendix D. Figure 1 shows the isotropic equivalent temperature factors for the cations in the White Well cordierite plotted against temperature. The Si atoms in the six-membered ring have the lowest temperature factors and increase at the slowest rate along with those outside the ring. The temperature factors for the Al atoms increase slightly faster, and at 24°C the M cations show the highest temperature factor and the greatest rate of increase to 775°C. The isotropic equivalents for the Dolni Bory cordierite are plotted against temperature in Figure 2. Despite the limited amount of data, the temperature factor variation with temperature for each cation has the same general trend as that observed for the White Well cordierite. These observations agree well with findings for the pyroxenes by Cameron *et al.* (1973) and for tremolite by Sueno *et al.* (1973). Both studies show that cations with higher charge and lower coordination have smaller temperature factors that increase more slowly with increasing temperature than cations with lower charge and higher coordination.

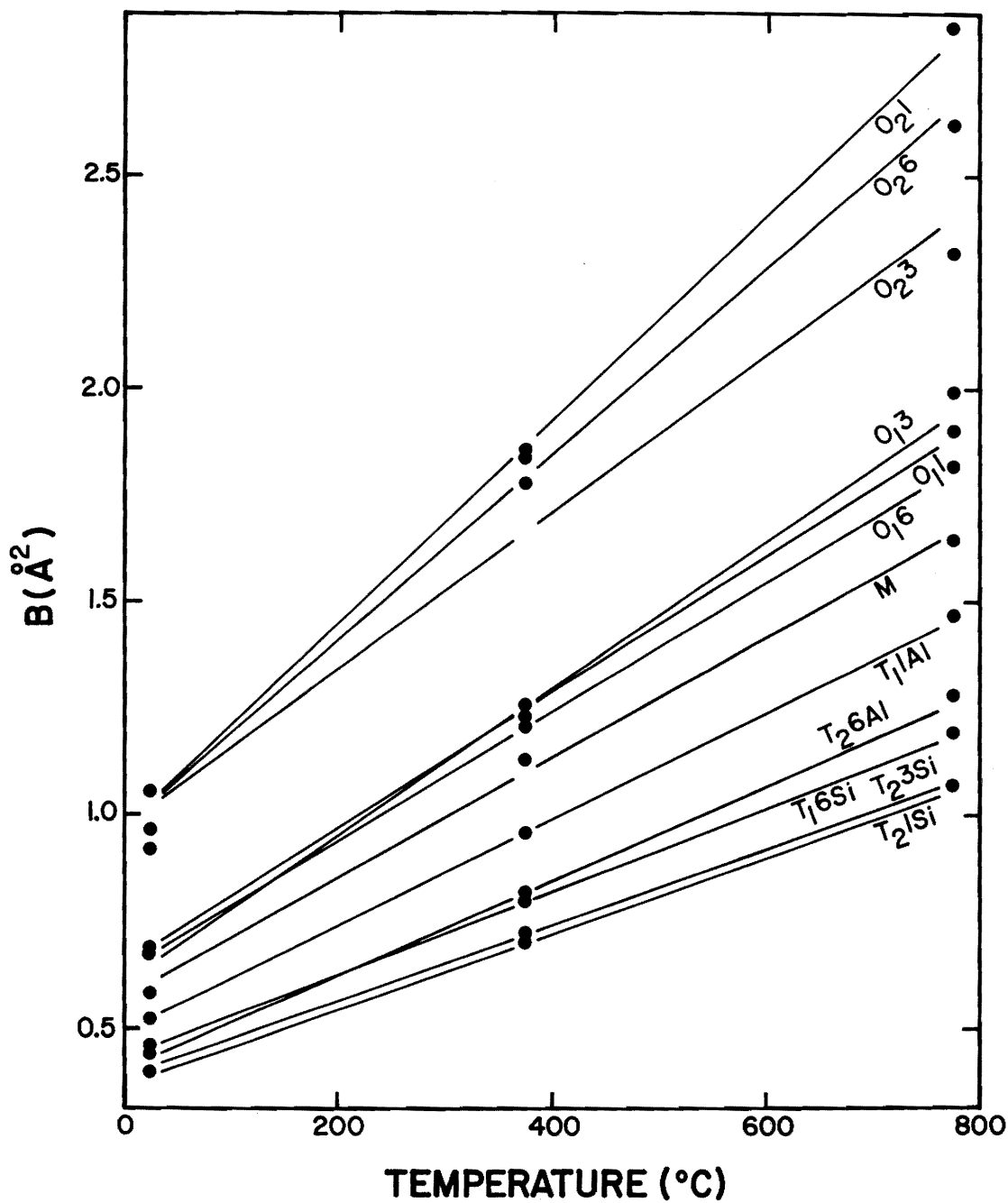


Figure 1. Isotropic equivalent temperature factors for the White Well cordierite plotted as a function of temperature from 24°C to 775°C. (The nomenclature of the atoms is the same as that in Fig. 4.)

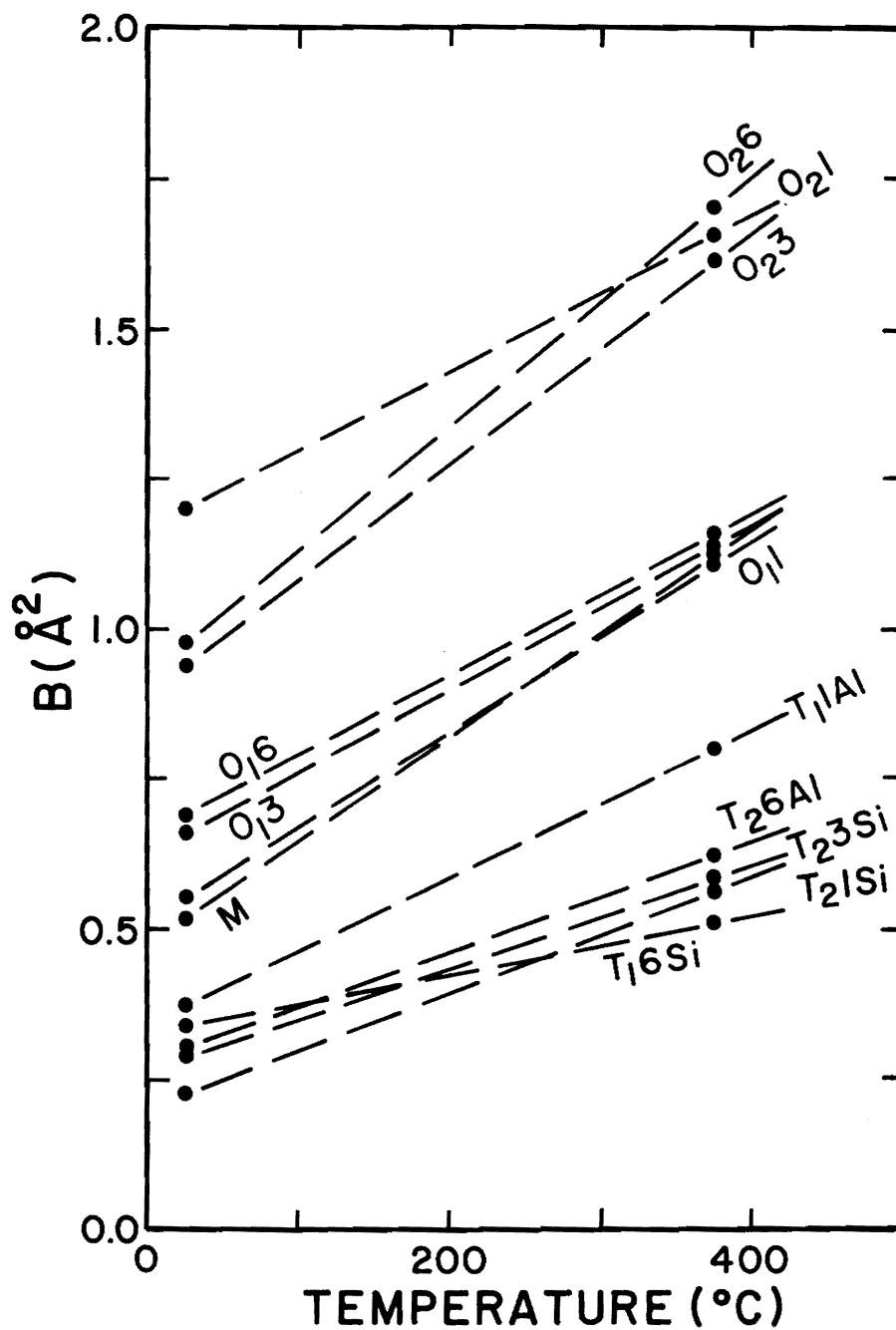


Figure 2. Isotropic equivalent temperature factors for the Dolni Bory cordierite plotted as a function of temperature from 24 $^{\circ}\text{C}$  to 375 $^{\circ}\text{C}$ . (The nomenclature of the atoms is the same as that in Fig. 4.)

The isotropic equivalent temperature factors of the oxygen atoms in the White Well cordierite are plotted against temperature in Figure 1. The six nonequivalent oxygens are clearly separated into two groups. The three distinct  $O_1$  oxygens are three-coordinated and have smaller temperature factors which increase at a slower rate than the three independent  $O_2$  oxygens in the ring which are only two-coordinated. Again, despite the limited data set, the oxygens in the Dolni Bory cordierite show the same general trends as evinced by the White Well cordierite (see Fig. 2). In general, oxygens with high coordination are more restricted in movement and display smaller temperature factors that increase slower with temperature. Oxygens with lower coordination seem to show the opposite trends as observed by Sueno *et al.* (1973) and Cohen *et al.* (1977).

#### *Cell Parameters*

The unit cell edges, obtained in a least-squares refinement of 28 computer centered reflections recorded at various temperatures up to 775°C for the White Well cordierite and up to 375°C for the Dolni Bory cordierite, are given in Table 3 along with their unit cell volumes and calculated distortion indices (Miyashiro, 1957).

The  $a$  cell edge of the White Well cordierite increases as a function of temperature at a rate slightly greater than that of  $b$  while  $c$  undergoes a slight but systematic shortening up to 775°C (Fig. 3). On the other hand, the  $c$ -cell edge of the Dolni Bory cordierite does not shorten upon heating but increases at about the same rate as the other axial directions. Because the changes in the

TABLE 3

Cell edges ( $\text{\AA}$ ), cell volume ( $\text{\AA}^3$ ), and calculated distortion index *vs* temperature for White Well cordierite

Temperature ( $^{\circ}\text{C}$ )	<i>a</i>	<i>b</i>	<i>c</i>	V	$\Delta$
24	17.088(3)	9.734(2)	9.359(1)	1556.7(4)	0.252
280	17.103(3)	9.737(2)	9.357(1)	1558.2(4)	0.262
375	17.113(3)	9.741(1)	9.358(1)	1560.0(3)	0.266
470	17.123(2)	9.745(1)	9.357(1)	1561.3(3)	0.268
590	17.132(2)	9.751(1)	9.357(1)	1563.1(3)	0.266
664	17.140(2)	9.755(1)	9.355(1)	1564.2(3)	0.267
775	17.149(2)	9.759(1)	9.352(1)	1565.1(3)	0.269
24*	17.119(2)	9.746(1)	9.361(1)	1561.8(3)	0.263

---

\* After heating

Cell edges ( $\text{\AA}$ ), cell volume ( $\text{\AA}^3$ ), and calculated distortion index *vs* temperature for Dolni Bory cordierite

Temperature ( $^{\circ}\text{C}$ )	<i>a</i>	<i>b</i>	<i>c</i>	V	$\Delta$
24	17.230(5)	9.835(3)	9.314(3)	1578.3(8)	0.211
375	17.258(3)	9.847(2)	9.328(2)	1585.3(3)	0.218

cell volume of the Dolni Bory cordierite are not as well determined as those of the White Well cordierite, it is difficult to directly compare the rates of volume expansion for the two cordierites.

The thermal expansion data for synthetic indialite measured by Fischer *et al.* (1974) and by Lee and Pentecost (1976) are compared with those for the White Well cordierite in Figure 3. The expansion of the  $a$ -cell edge of the ordered White Well cordierite is about 1500 ppm greater at 775°C than that of indialite whereas the expansion along  $b$  is practically the same as that along  $a$  in the disordered polymorph. The contraction along  $c$  in the White Well cordierite is significantly less ( $\sim$ 800 ppm less at 775°C) than that along  $c$  in indialite. Moreover, the variation of  $c$  in the ordered polymorph is linear with temperature within the limits of error of the result. The two measurements for the disordered polymorph show a contraction along  $c$  with temperature, but Fischer *et al.* (1974) find that  $c$  begins to expand at temperatures greater than  $\sim$ 400°C whereas Lee and Pentecost (1976) find that  $c$  continues to contract up to 1000°C. However, when Lee and Pentecost (1976) annealed their hexagonal specimen to produce an orthorhombic polymorph (with greater degree of order), they discovered that the contraction along  $c$  was increased over that of the hexagonal polymorph. Since the degree to which long-range order may develop in indialite is probably variable (Meagher and Gibbs, 1977) and since the contraction properties in the direction of  $c$  apparently depend on thermal history and structural state, we believe that the differences in the curves determined by Fischer *et al.* (1974) and Lee and Pentecost (1976) are real and

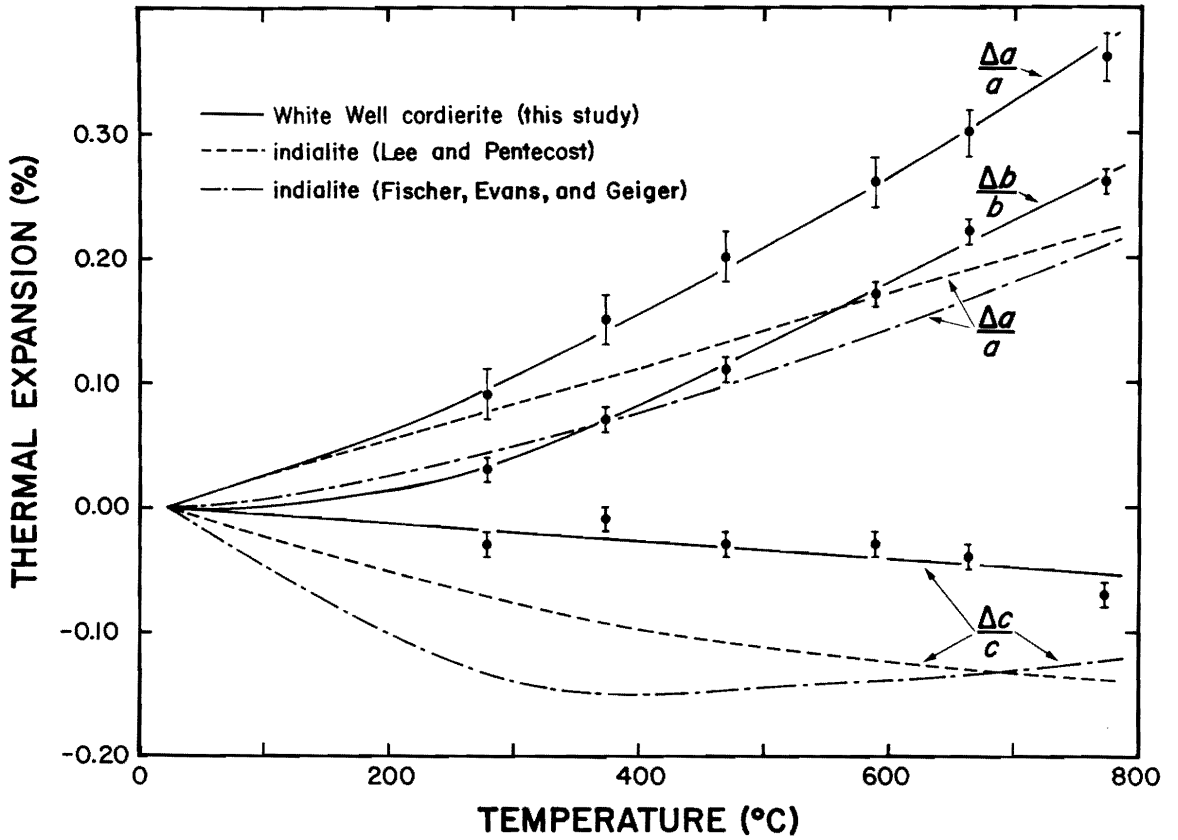


Figure 3. Axial expansion ( $[(X_T - X_{24})/X_{24}] \cdot 100$  where X is a, b or c) vs temperature for two synthetic indialites and the White Well cordierite. The brackets for the White Well data are drawn at  $1\hat{\sigma}$ .



represent measurements on hexagonal polymorphs with different structural states.

## STRUCTURE

The crystal structure of cordierite is described by Takane and Takeuchi (1936), Byström (1942), Gibbs (1966), Cohen *et al.* (1977) and Meagher and Gibbs (1977), and consists of a framework of four- and six-membered rings of tetrahedra. The six-membered rings lie in planes perpendicular to  $c$  and involve the three nonequivalent  $T_2$  tetrahedra (see Fig. 4). The four-membered rings, consisting of alternating  $T_1$  and  $T_2$  tetrahedra, are linked into chains paralleling  $c$  which are further cross-linked to form the tetrahedral framework (see Fig. 5). A neutron site refinement by Cohen *et al.* (1977) has shown the White Well cordierite to be completely ordered ( $t_{16} = t_{21} = t_{23} = 0.0$  and  $t_{11} = t_{26} = 1.0$  where  $t_{xy}$  represents the probability of finding an Al atom in  $T_{xy}$ ) within the experimental error. On the other hand, an examination of the mean T-O bond lengths determined in an X-ray study of indialite indicates that the crystal has a long-range order of 0.38 with  $t_1 = 0.72$  and  $t_2 = 0.30$  (Meagher and Gibbs, 1977). The M-atoms (M = Mg, Fe) in cordierite reside within the framework in somewhat flattened octahedra that share two edges with  $AlO_4$  tetrahedra and one with a  $SiO_4$  tetrahedron. The large cavities, connected one to another by the openings of the six-membered rings, house the water molecules in hydrous cordierite with the alkali atoms residing at the origin and centering the six-membered rings of  $T_2$ -tetrahedra (Meagher, 1967).

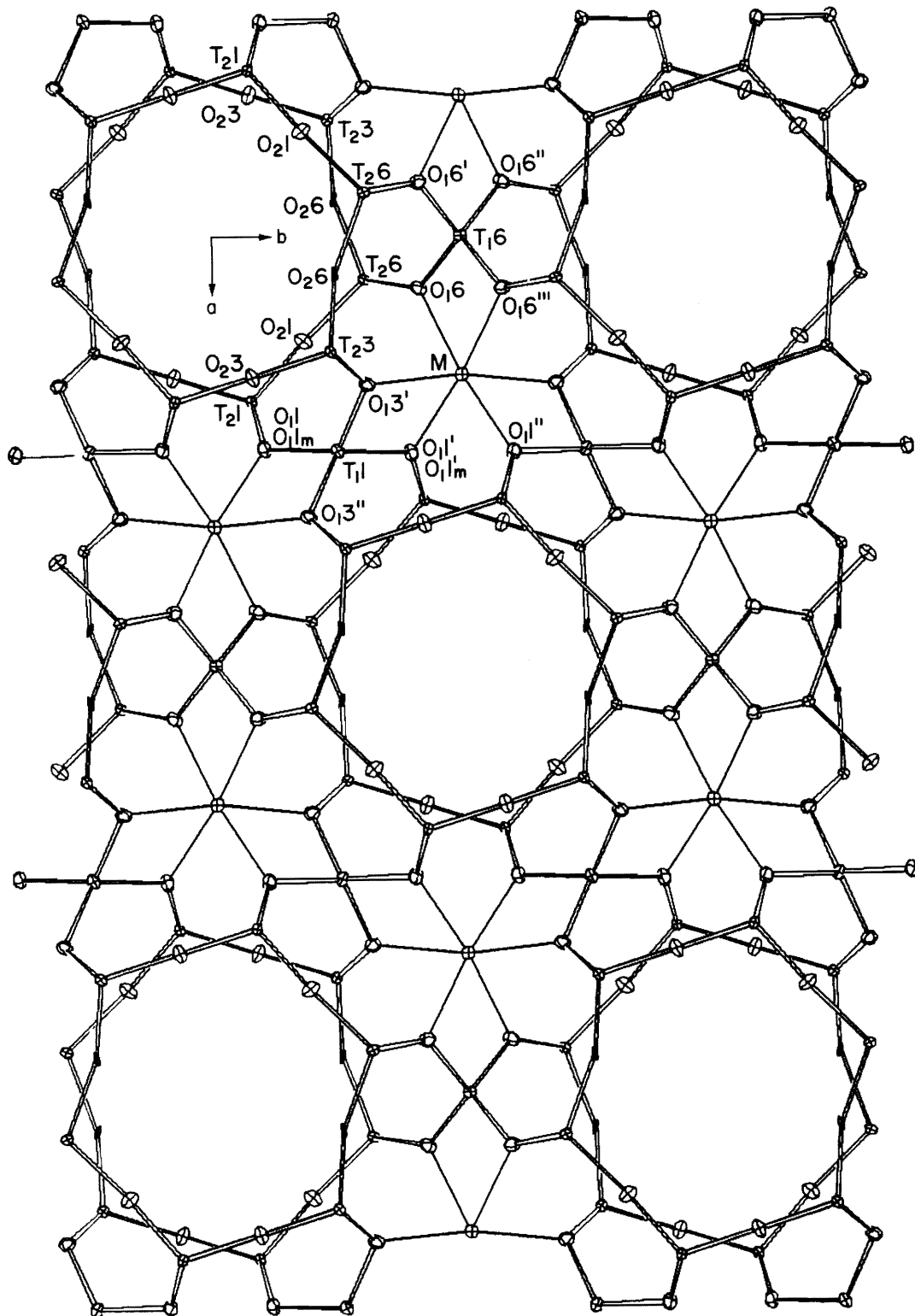


Figure 4. ORTEP (Johnson, 1965) drawing of the cordierite structure (between  $0c$  and  $1/2c$ ) viewed down  $c$ . In ordered cordierite,  $T_{11}$  and  $T_{26}$  represent Al atoms, while  $T_{16}, T_{21}$ , and  $T_{23}$  represent Si atoms. The M octahedra houses Mg and Fe.

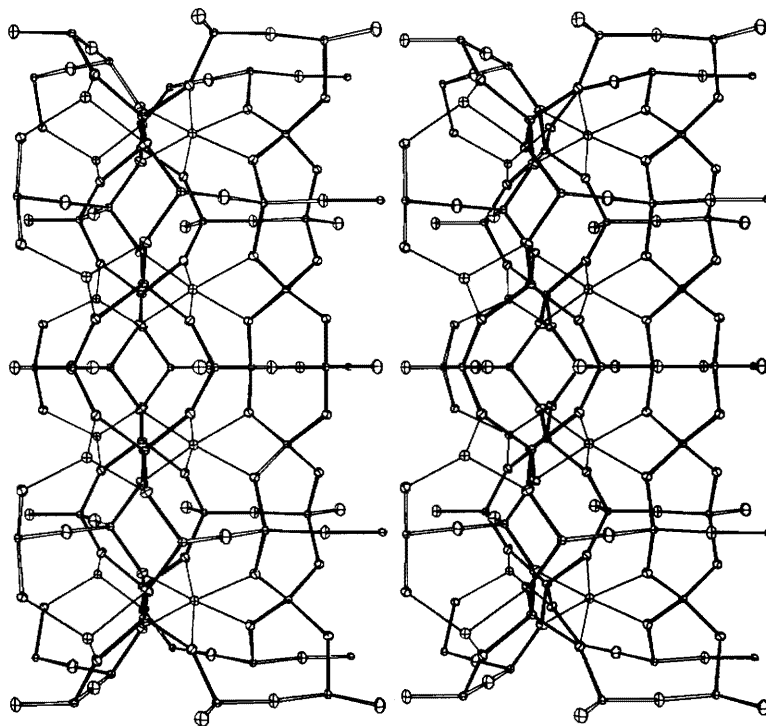


Figure 5. An ORTEP stereopair drawing showing the four-membered rings which are linked into chains paralleling  $c$ . The two symmetrically distinct chains are shown (the two overlying chains on the left are related by a  $c$ -glide) and have been highlighted by heavy-lined bonds. Note that the octahedron (single line bonds) shares three edges with tetrahedra. In this figure,  $a$  is horizontal and  $c$  is vertical.

## DISCUSSION

### *Tetrahedral and Octahedral Bond Length Expansion*

The mean T-O bond lengths for the individual tetrahedra in both the White Well and the Dolni Bory cordierites do not appear to change significantly with temperature, nor are they different after heating in the case of the White Well cordierite. Accordingly, we may conclude that the ordered configuration of Al and Si in the tetrahedral framework of low cordierite was unaffected by our heating experiments. On the other hand, the octahedral M-O bonds show a significant increase in length. The Mg-O bonds in the White Well cordierite increase 0.018 Å on the average when heated from 24°C to 775°C while the Fe-O bonds in the Dolni Bory cordierite increase by 0.007 Å when heated from 24°C to 375°C. Hence, in the temperature range 24°C to 375°C, the mean Fe-O bond length expansion ( $\sim 0.007(1)$  Å) is less than that of the mean Mg-O bond length expansion ( $\sim 0.011(1)$  Å). This result indicates that the Fe-O bond is stronger than the Mg-O bond, in agreement with similar results obtained by Skinner (1966) and Cameron *et al.* (1973).

Because the mean T-O bond lengths appear to remain unchanged, the volumes of the  $AlO_4$  and  $SiO_4$  tetrahedra show little change with heating (see Table 4). In contrast, the  $MgO_6$  octahedra in the White Well cordierite exhibit a volume increase of  $0.27 \text{ \AA}^3$  when heated from 24°C to 775°C. Similarly, the  $FeO_6$  octahedra in the Dolni Bory cordierite show a volume increase of  $0.13 \text{ \AA}^3$  when heated to 375°C.

TABLE 4

Polyhedral volumes ( $\text{\AA}^3$ ) vs temperature for  
White Well cordierite

Polyhedra	24°C	375°C	775°C	24°C*
T <sub>1</sub> 1	2.58	2.57	2.58	2.59
T <sub>1</sub> 6	2.14	2.13	2.15	2.13
T <sub>2</sub> 1	2.15	2.16	2.15	2.17
T <sub>2</sub> 6	2.70	2.72	2.72	2.72
T <sub>2</sub> 3	2.16	2.16	2.17	2.16
M	11.79	11.91	12.06	11.86

---

\* After heating

Polyhedral volumes ( $\text{\AA}^3$ ) vs temperature  
for Dolni Bory cordierite

Polyhedra	24°C	375°C
T <sub>1</sub> 1	2.61	2.63
T <sub>1</sub> 6	2.16	2.17
T <sub>2</sub> 1	2.18	2.17
T <sub>2</sub> 6	2.73	2.72
T <sub>2</sub> 3	2.16	2.17
M	12.42	12.55

The mean thermal expansion of the octahedron in the Mg-rich cordierite ( $12.6 \times 10^{-6} \text{ } ^\circ\text{C}^{-1}$ ) is significantly less than that observed for corresponding octahedra in periclase ( $13.9 \times 10^{-6} \text{ } ^\circ\text{C}^{-1}$ ), forsterite ( $14.2 \times 10^{-6} \text{ } ^\circ\text{C}^{-1}$ ) and diopside ( $14.4 \times 10^{-6} \text{ } ^\circ\text{C}^{-1}$ ) (Hazen and Prewitt, 1977). As indicated earlier, the octahedron in cordierite is isolated from other octahedra and shares three of its edges with tetrahedra. Since the dimensions of these tetrahedra show little or no change with heating, they act as rigid clamps and constrain the octahedron in its expansion upon heating. The octahedra in forsterite and diopside share edges with both tetrahedra and octahedra, those in periclase just sharing edges with other octahedra. The mutual expansion of the octahedra in these structures should not be as restricted. If this is true, then the mean thermal expansion of an M-containing polyhedron depends upon its environment as well as the strength of the M-O bond.

When trying to predict the thermal expansion of a crystalline material from its structure, which as Kahn (1976) points out, has "met with limited success," it may be inappropriate to assign a fixed rate of expansion to an M-O bond from one structure type to another.

#### *A Structural Interpretation of the Thermal Expansion of Cordierite*

The anisotropic thermal expansion of the unit cell of the White Well cordierite may be related to the thermal expansion of its Mg-rich octahedron and its accompanying effect on the tetrahedral framework. Figure 6 shows that the volume change of the octahedron correlates linearly with  $a$  and  $b$ , both axial directions increasing as the octahedral volume increases upon heating. On the other hand,

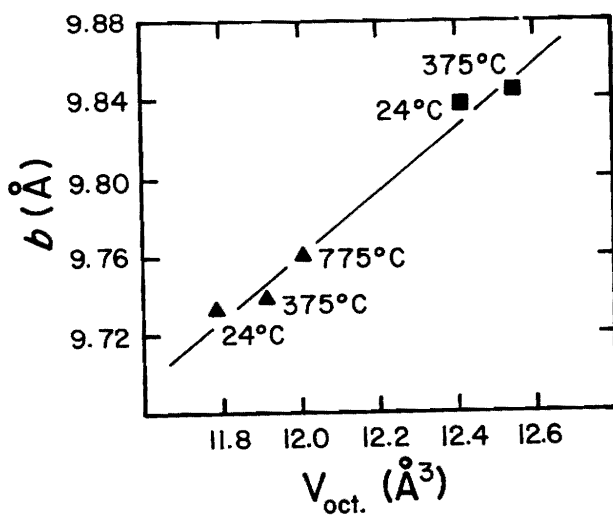
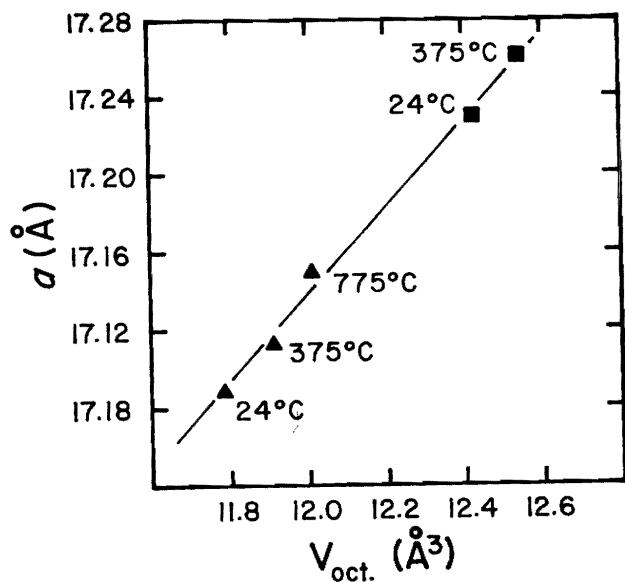


Figure 6. The  $a$  and  $b$  cell edges vs the octahedral volume for both the White Well ( $\blacktriangle$ ) and Dolni Bory ( $\blacksquare$ ) cordierites at various temperatures. The relationships between the cell edges and the octahedral volumes are similar for both cordierites and seem to be continuous as shown by the linearity of the data points.



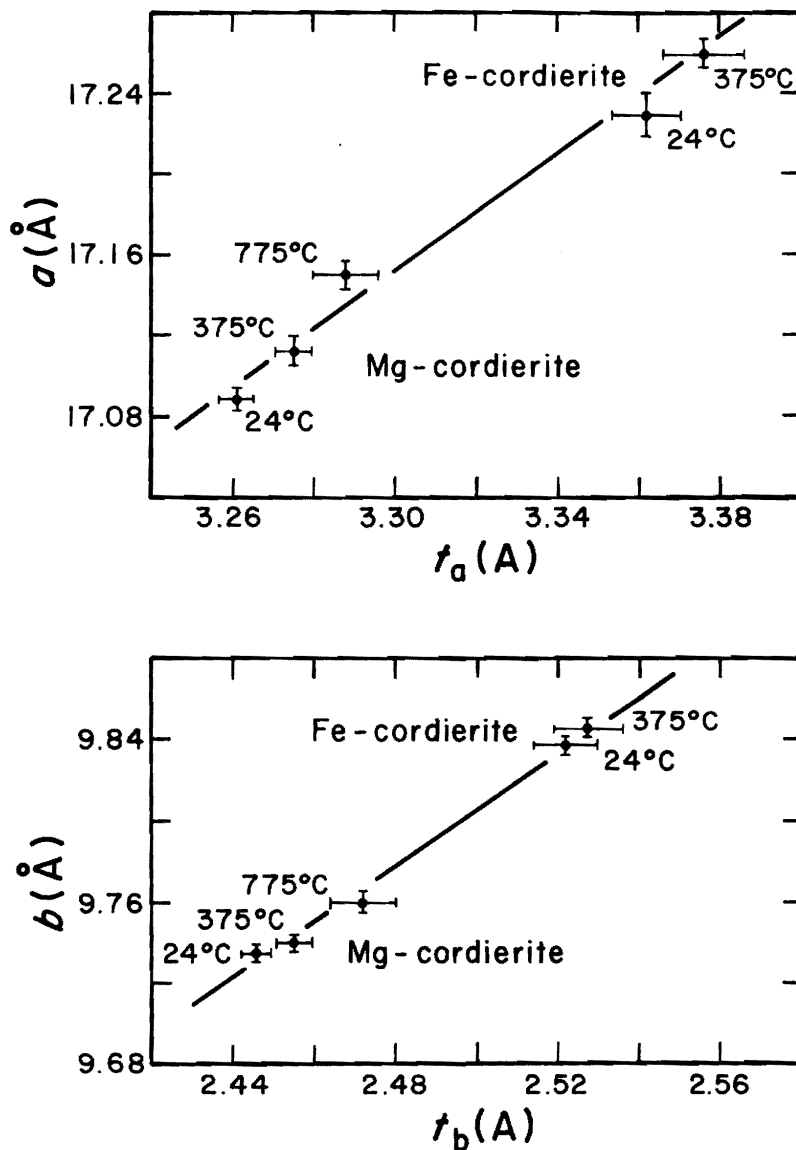


Figure 7. The  $a$  and  $b$  cell edges vs the thickness of the M-octahedron measured along  $a$ ,  $t_a$ , and along  $b$ ,  $t_b$ , for the White Well (Mg) and Dolni Bory (Fe) cordierites at various temperatures. The relationships between  $a$  and  $b$  and  $t_a$  and  $t_b$  are similar for both cordierites and seem to be continuous as shown by the linearity of the data points. The brackets are drawn at  $1\hat{\sigma}$ .

the  $c$ -cell edge appears to be independent of the volume change. In addition, the associated changes in the thickness of the octahedron measured along  $a$  and  $b$  correlate with changes in the lengths of  $a$  and  $b$  (Fig. 7) while the octahedral thickness measured along  $c$  is unaffected by the temperature change. This anisotropic expansion of the octahedron serves to rotate ( $\sim 0.2^\circ$ ) the rigid six-membered rings clockwise and counterclockwise in alternate layers perpendicular to  $c$  (Fig. 8). Figure 9 shows the displacements of each of the tetrahedral cations in the rings accompanying this rotation. The twisting of the tetrahedral framework attending the rotation may be associated with a decrease in selected T-O-M and O-T-O angles which results in a more efficient packing of the structure and a concomitant contraction of the  $c$ -cell edge (Fig. 10).

As a test of the assertion that the thermal expansion of the octahedron is the driving force behind the thermal expansion of cordierite, we completed a *DLS* (Meier and Villiger, 1969) calculation (Meagher, Hochella and Gibbs, in preparation) for the White Well cordierite. The T-O bond lengths used in the calculation were initially set at the room temperature values ( $24^\circ\text{C}$ ) and the M-O bond lengths and the cell edges were initially set at the values measured at  $775^\circ\text{C}$ . The results of the calculation (Appendix E) show a close correspondence with the bond lengths and angles measured for the cordierite at  $775^\circ\text{C}$ , *i.e.*, almost all are within one or two estimated standard deviations of those recorded for the observed structure. This result agrees with the assertion that the anisotropic thermal expansion of the unit cell of cordierite is controlled in part by

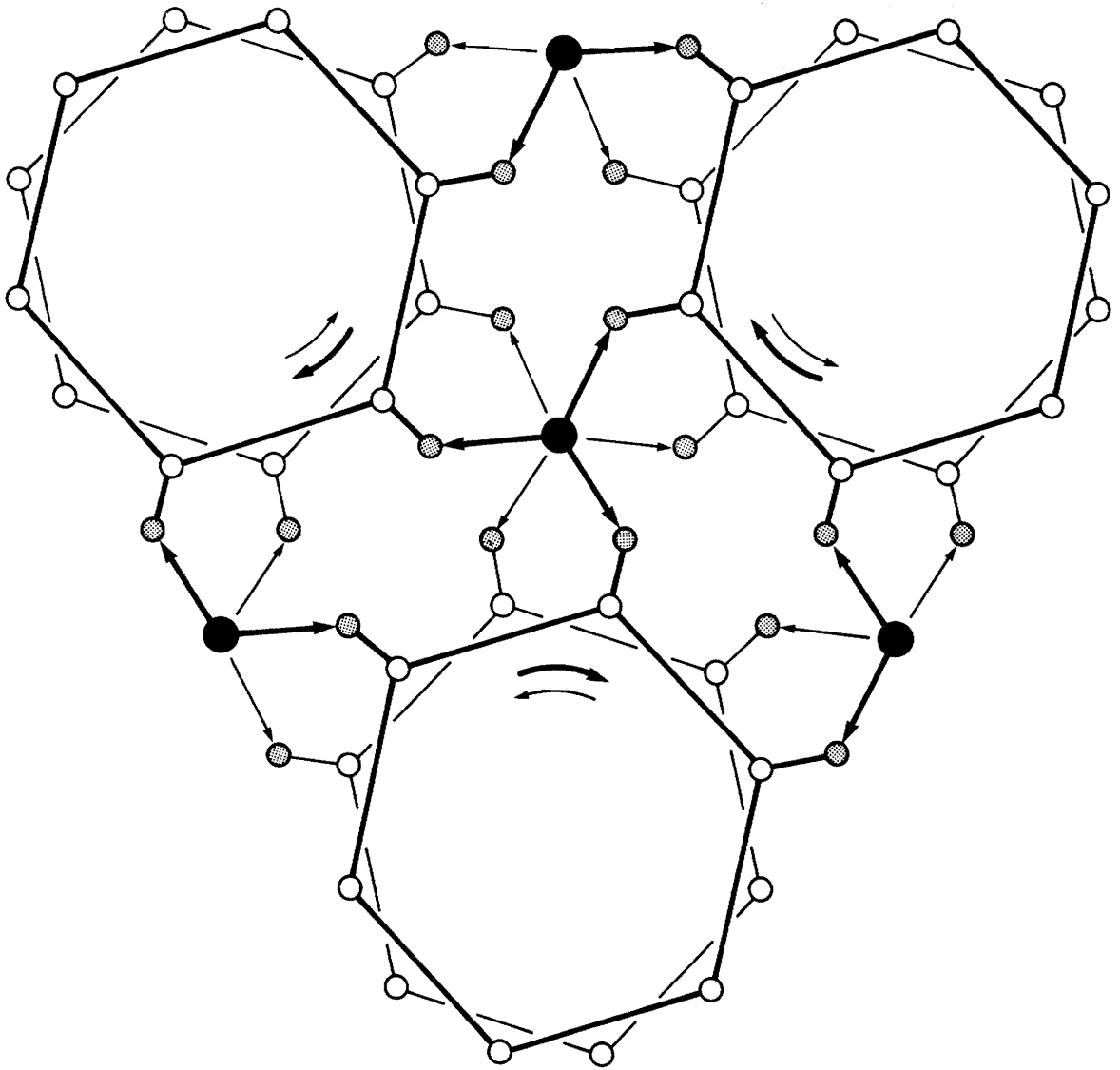


Figure 8. Rotation of the six-membered rings in the White Well cordierite. The open circles represent the tetrahedral cations in the ring, the dotted circles the  $O_1$  oxygens, and the solid circles the octahedral cations (96% Mg). The vectors represent the expanding Mg-O bonds. The upper six-membered rings rotate upon heating in a clockwise direction whereas the lower ones rotate in a counterclockwise direction.

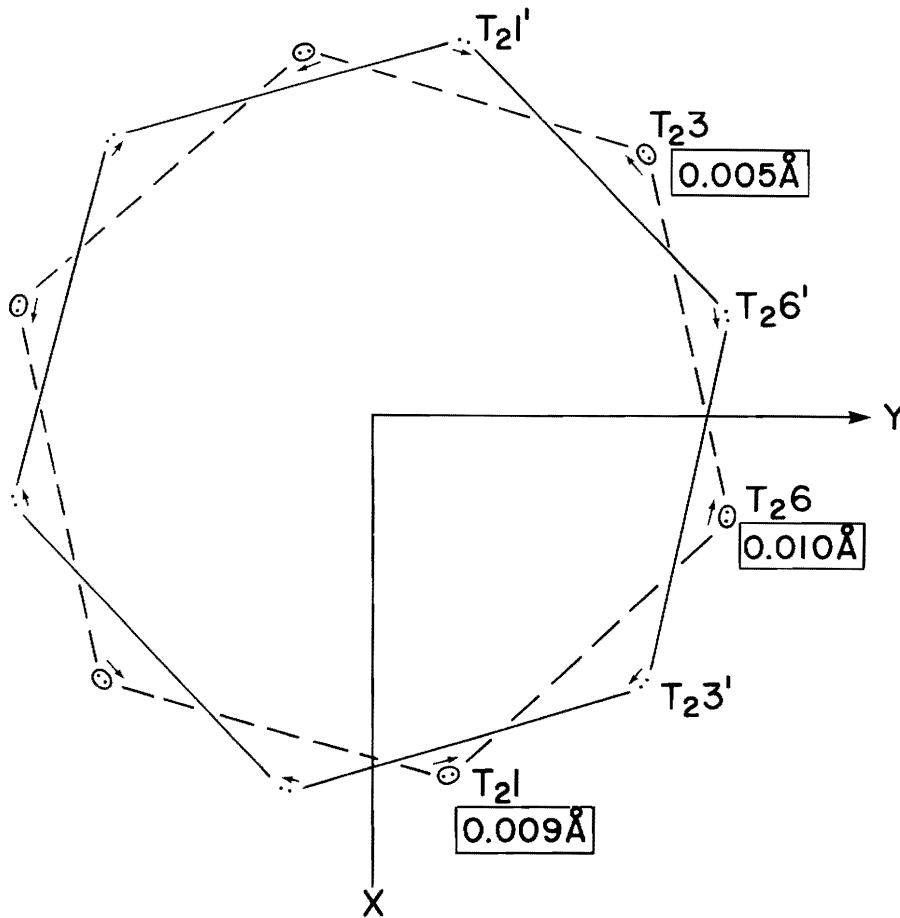


Figure 9. Stereographic projection of the actual displacements (boxes) of the independent tetrahedral ring cations from 24°C to 775°C in the White Well cordierite. The direction of rotation of these rings corresponds to the scheme shown in Figure 8, the upper ring rotating clockwise, the lower counterclockwise. The upper and lower rings are related by a 2-fold along Y as shown.

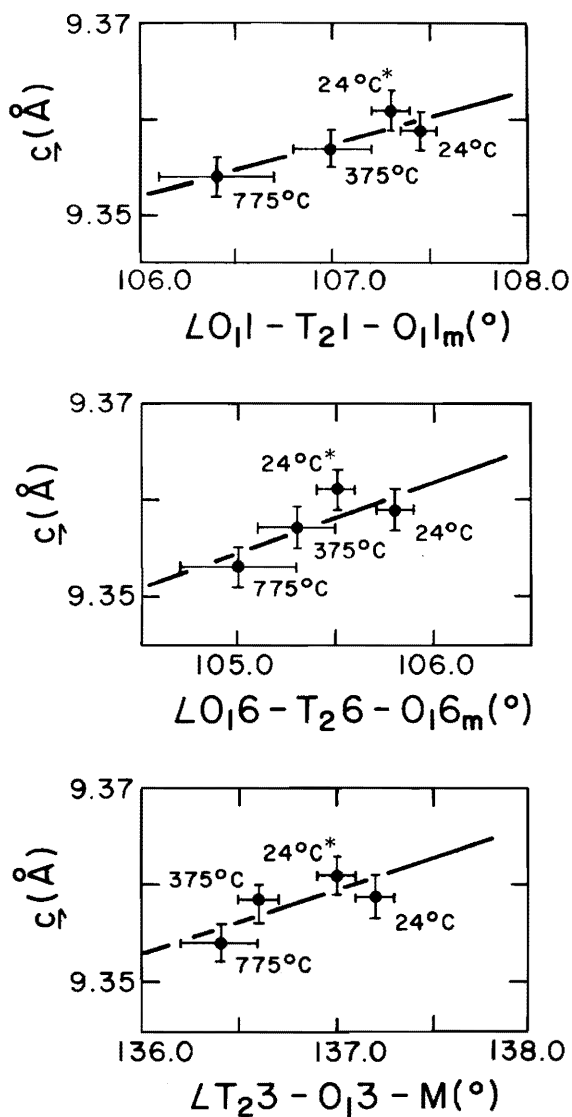


Figure 10. The length of the  $c$ -cell edge vs one T-O-M and two O-T-O angles at various temperatures for the White Well cordierite. These angles are oriented such that their change directly affects  $c$ . Their decrease is apparently related to the expansion of the octahedral bonds and slight rotation of the rings. Error bars are drawn at  $1\hat{\sigma}$ . (24°C\* is after heating.)

the anisotropic thermal expansion properties of the octahedron.

The relationships between the thermal expansion of the Fe-rich octahedron and the  $a$ - and  $b$ -cell edges of the Dolni Bory cordierite is practically the same as that measured for the White Well cordierite (Figs. 6 and 7). The thickness of the octahedron measured along  $a$  and  $b$  is significantly greater than that measured for the White Well cordierite which conforms with the larger  $a$  and  $b$  cell dimensions of the Dolni Bory cordierite. Also, like the White Well cordierite, the change in the thickness of the octahedron measured along  $a$  and  $b$  correlates with the changes in these cell dimensions. However, despite the larger volume of the Fe-octahedron, the  $c$ -cell edge of the Dolni Bory cordierite is  $0.05 \text{ \AA}$  shorter than that measured for the White Well cordierite. In addition, the thickness of the Fe-rich octahedron is significantly less than that of the Mg-rich octahedron, both measured along  $c$ . Unlike the White Well cordierite, both the thickness of the octahedron and the  $c$ -cell edge of the Dolni Bory cordierite increase with rising temperature. Also, evidence is lacking in support of a rotation of the six-membered rings associated with the expansion of the octahedron up to  $375^\circ\text{C}$ .

#### *Orientation of the Water Molecules in the White Well Cordierite*

A re-investigation of the water position in the channels of the White Well cordierite as proposed by Cohen *et al.* (1977) has led to a new, but not complete, interpretation using the X-ray and neutron diffraction data of Cohen (1975). X-ray  $\Delta\rho$  maps show the oxygen of the water molecule (Ow) to be split into two positions along the  $x$  axis at  $\pm 0.027, 0, 1/4$  as shown in Figure 11. Neutron  $\Delta\rho$  maps (see

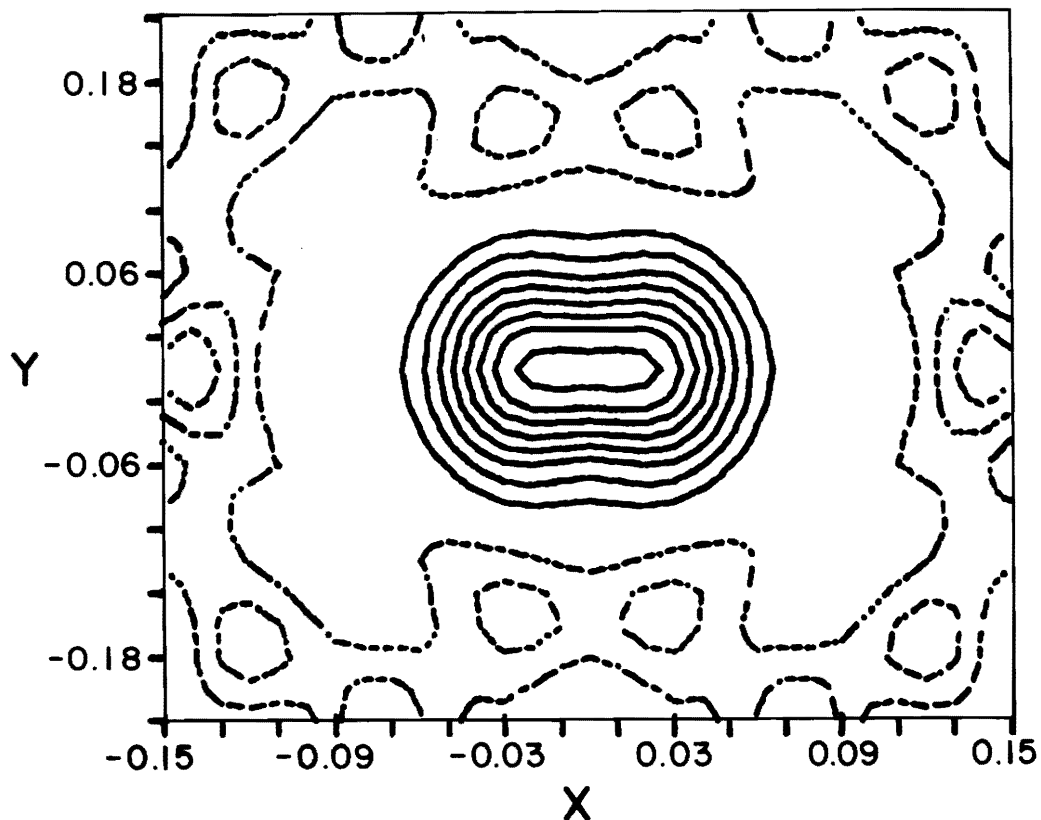


Figure 11. X-ray  $\Delta\rho$  map (24°C) showing the elongated oxygen peak along the x axis. Section is the 001 plane at  $z = 1/4$ . The contour interval is  $.20e^{-}/\text{\AA}^3$  and the zero contour has been omitted. Subtraction of the peak was most complete when electron density was added at  $\pm.027$  on x.

Fig. 12) strongly suggest that there is an H-O-H position near the 100 plane with the H-H vector  $23^\circ$  from  $c$ . This  $H_2O$  position essentially agrees with the orientation of the water molecule proposed by Farrell and Newnham (1967), Tsang and Ghose (1972) and the type I water of Goldman *et al.* (1977), all based on spectroscopic methods. Problems arose when we attempted to completely subtract out the  $Ow$  peak using the multiplicity of  $H_2O$  from the chemical analysis of the White Well cordierite (Pryce, 1973). A negative residual was left at the  $Ow$  position indicating that the amount of  $H_2O$  in the formula should be  $(H_2O)_{.36}$  instead of  $(H_2O)_{.56}$ . To further support the idea that less water is present, the amount of hydrogen needed to diminish the negative peaks of the  $\Delta\rho$  map in Figure 12 fits with  $(H_2O)_{.36}$ . However, a thermal gravimetric weight loss curve for the White Well cordierite suggests that the amount of  $H_2O$  in the formula is correct. Despite this puzzling result, there is no evidence in these maps for the type II  $H_2O$  (H-O-H in the 100 plane with the H-H vector parallel to  $b$ ) proposed by Goldman *et al.* (1977).

#### *The Effects of Heating on Channel Constituents*

The loosely bound channel constituents in cordierite undergo large anisotropic vibrations and positional changes upon heating. Four  $\Delta\rho$  maps at each temperature of refinement (Figs. 13a-d) illustrate this in the White Well cordierite. The peak ascribed to the alkali atoms at 0,0,0 is elongated parallel to  $c$ , the channel axis, at  $375^\circ C$ , while the  $Ow$  peak seems to have become a single peak at 0,0,1/4 elongated further along  $a$  than the double peak at  $24^\circ C$ .



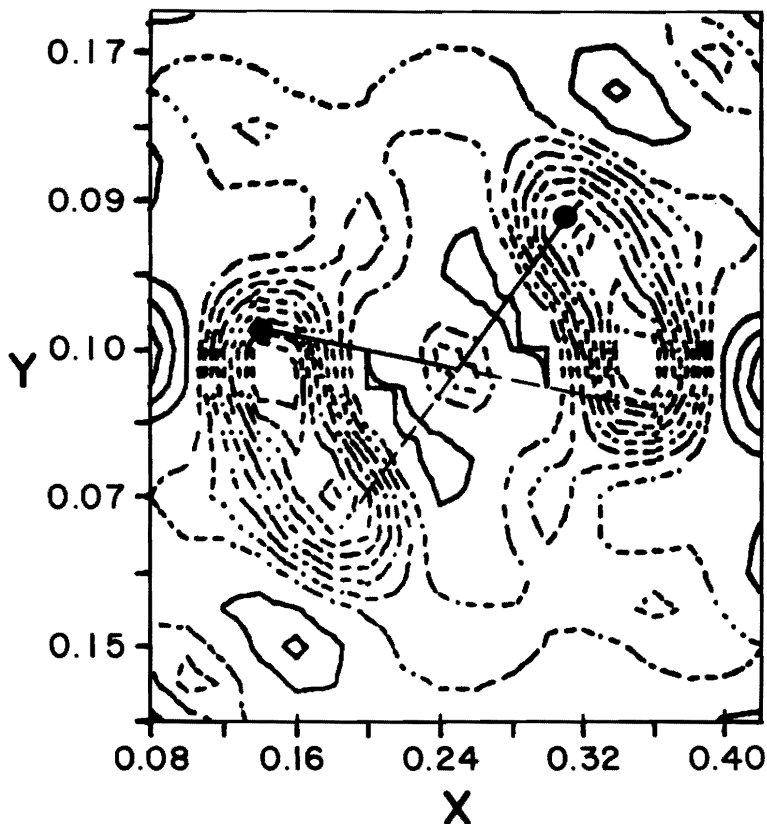


Figure 12. Neutron  $\Delta\rho$  map ( $24^\circ\text{C}$ ) showing the negative scattering of the hydrogens (zero contour omitted) in the 100 plane at  $x = .01$ . The  $\text{Ow}$  peak has been subtracted out. The geometry of the 2 symmetry related water molecules shown is  $d(\text{H1-Ow}) = 0.99 \text{ \AA}$ ,  $d(\text{H2-Ow}) = 1.01 \text{ \AA}$  and  $\angle\text{H1-Ow-H2} = 105.1^\circ$  with H1 at  $x = .010$ ,  $y = .025$ ,  $z = .150$ , H2 at  $x = .010$ ,  $y = .078$  and  $z = .311$  and  $\text{Ow}$  at  $x = .027$ ,  $y = 0$ ,  $z = 1/4$ .

At 775°C in the White Well cordierite, the Ow peak is absent only to reappear in the 24°C (after heating)  $\Delta\rho$  map as a single peak, less than half the size of the original Ow peak. This peak is no longer elongated parallel to  $\alpha$ . The absence of the peak at 775°C is probably due to the water molecule's high temperature factors and seemingly complete disorder within the cavity. The Ow peak vanishes similarly in the Dolni Bory cordierite in the  $\Delta\rho$  map computed from the 375°C data. On the other hand, the peak centering the six-membered ring has enlarged in the 775°C  $\Delta\rho$  map for the White Well cordierite. Also, in the 24°C (after heating)  $\Delta\rho$  map, it is clear that there is more electron density at 0,0,0 than the unheated sample, less electron density at 0,0,1/4, and an overall substantial drop in the original amount of channel constituents. It seems reasonable to suggest that some of the channel constituents have been driven out of the structure, while some of the remaining H<sub>2</sub>O molecules have taken up positions centering the six-membered ring.

#### *The State of the White Well Cordierite After Heating*

The  $a$ - and  $b$ -cell edges of the White Well cordierite do not return to their original lengths after cooling to 24°C (Table 3). Observations such as these are usually attributed to a change in structural state with heating (see, for example, Karkhanavala and Hummel (1953) and Levien and Papike (1976)). However, this is not the case for the White Well cordierite since its completely ordered structure did not disorder at all during data collection at high temperatures. Possible explanations might include secondary

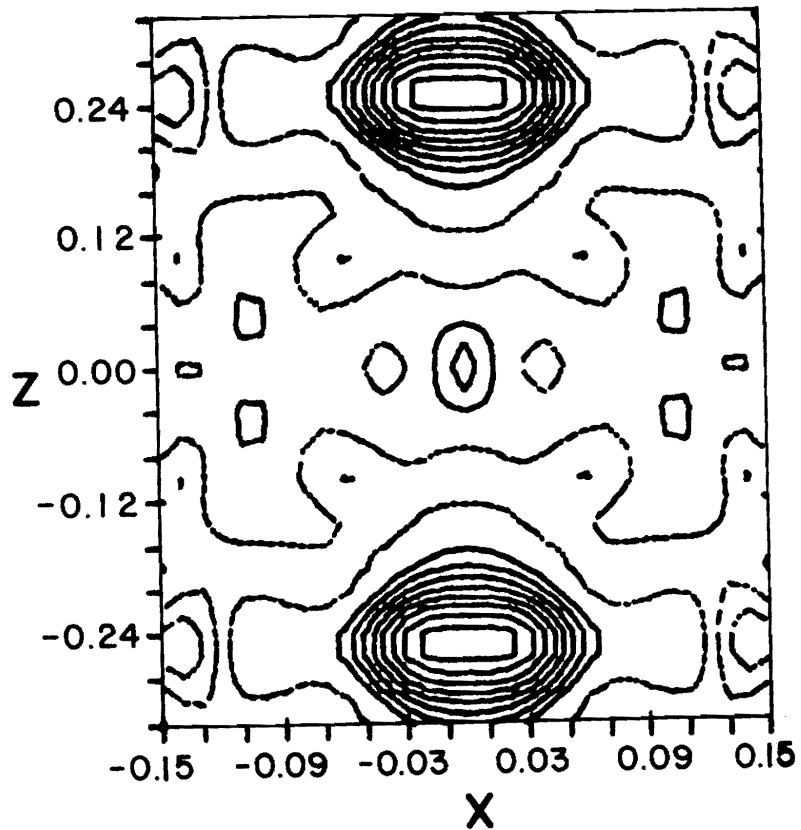


Figure 13a. X-ray  $\Delta\rho$  map of the White Well cordierite showing the peaks ascribed to the channel constituents at 24°C. The zero contour is omitted and the contour interval is  $.20e^{-}/\text{\AA}^3$ .

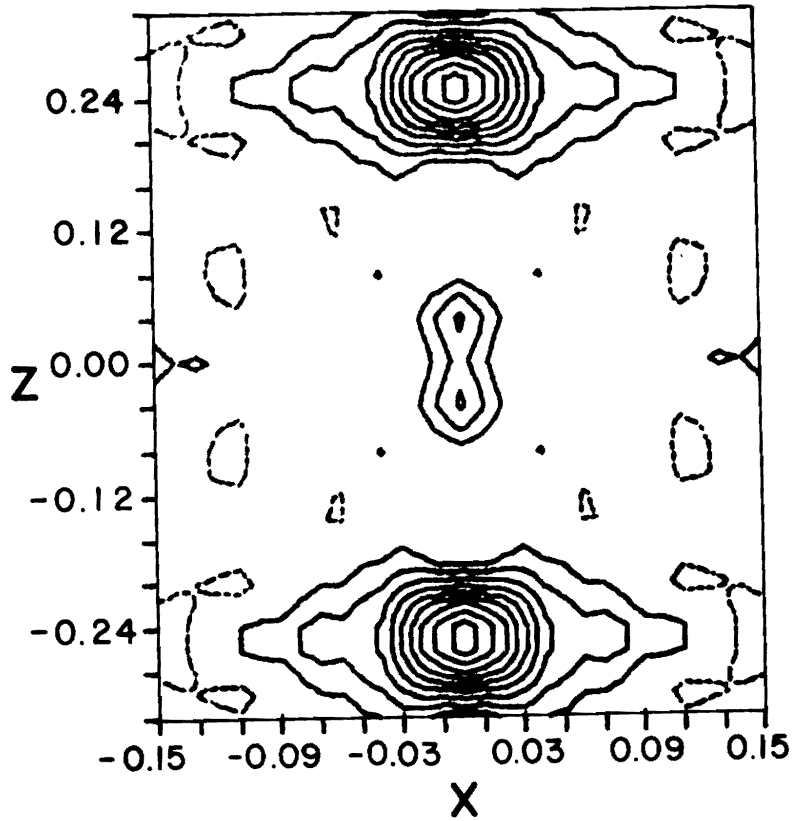


Figure 13b. X-ray  $\Delta\rho$  map of the White Well cordierite showing the peaks ascribed to the channel constituents at 375°C. The zero contour is omitted and the contour interval is  $.20e^-/\text{\AA}^3$ .

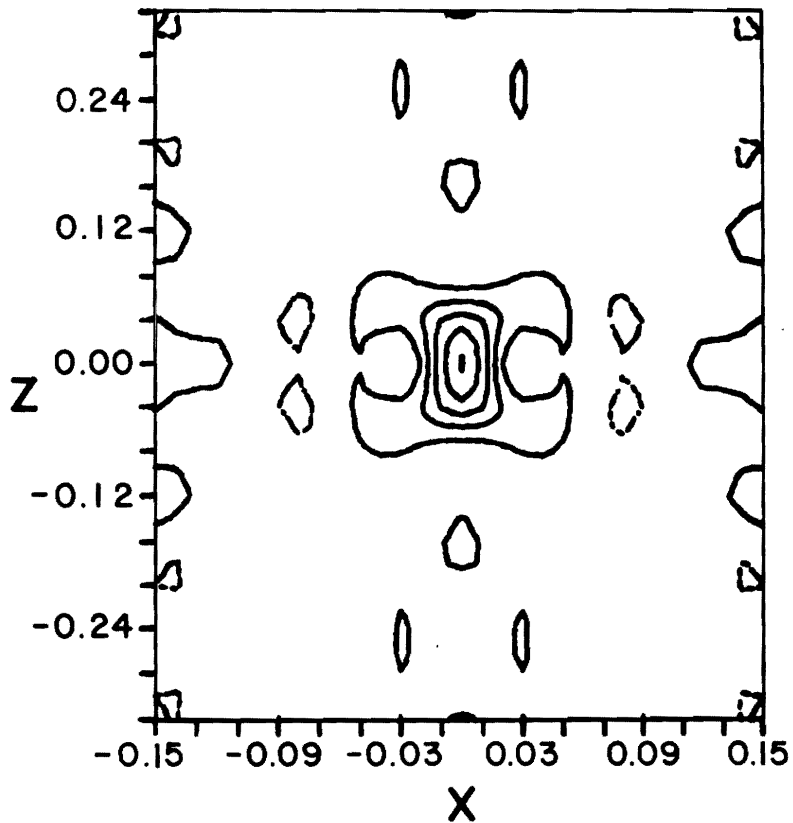


Figure 13c. X-ray  $\Delta\rho$  map of the White Well cordierite showing the peaks ascribed to the channel constituents at 775°C. The zero contour is omitted and the contour interval is  $.20e^{-/\text{\AA}^3}$ .

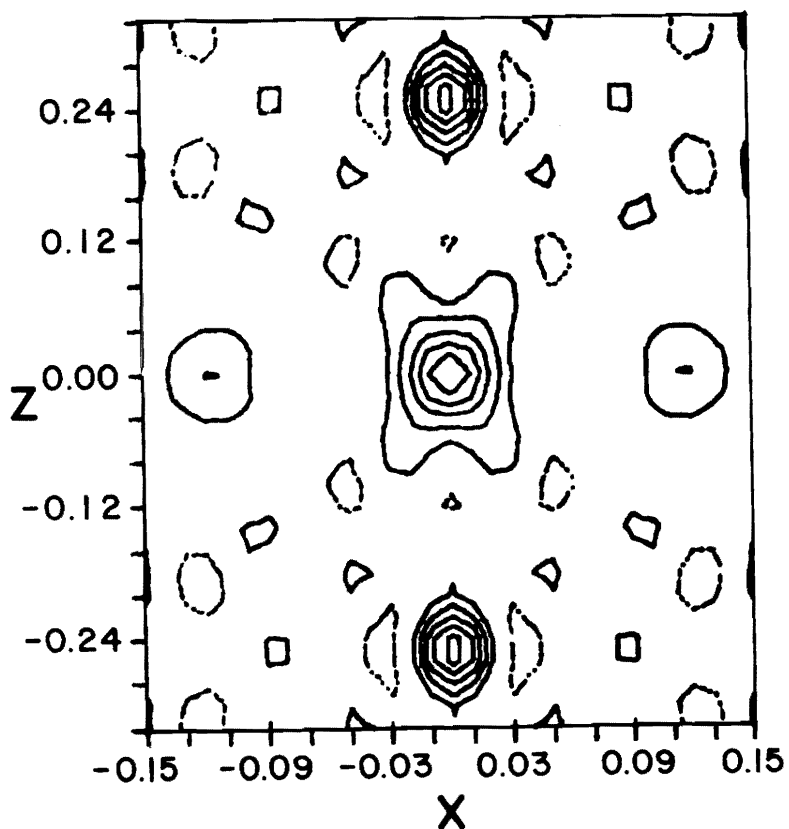


Figure 13d. X-ray  $\Delta\rho$  map of the White Well cordierite showing the peaks ascribed to the channel constituents at 24°C (after heating). The zero contour is omitted and the contour interval is  $.20e^{-}/\text{\AA}^3$ .

hematite forming upon heating or the channel constituents changing in amount and perhaps position with heating and cooling as shown in the previous section. It is not clear, though, how these changes might affect the  $\text{Al}_4\text{Si}_5\text{O}_{18}$  framework, if at all (see Langer and Schreyer (1976) and Stout (1976)). Another, more plausible, explanation would seem to be that some of the iron in the framework was used to form the secondary hematite, and as a result some of the octahedra were left empty. Octahedral vacancies take up more space than filled octahedra, and  $a$  and  $b$  would be appropriately larger (see Table 4 and Fig. 6). If octahedral vacancies existed in the framework after heating, one would expect the isotropic temperature factors of the octahedra to be less after heating than before. But again this is not the case (see Appendix D). Thus, this question remains unresolved pending further study.

## REFERENCES

- BLOSS, F.D. (book in preparation) *The Spindle Stage: Principles and Practice*.
- BROWN, G.E., S. SUENO, and C.T. PREWITT (1973) A new single-crystal heater for the precession camera and four-circle diffractometer. *Am. Mineral.* 58, 698-704.
- BYSTRÖM, A. (1941) Crystal structure of cordierite. *Arkiv. Kemi, Min. Geol.* 15B, No. 12, 7 pp.
- CAMERON, M., S. SUENO, C.T. PREWITT, and J.J. PAPIKE (1973) High-temperature crystal chemistry of acmite, diopside, hedenbergite, jadeite, spodumene, and ureyite. *Am. Mineral.* 58, 594-618.
- COHEN, J.P. (1975) *An X-ray and Neutron Diffraction Study of Hydrous Low Cordierite*. M.S. Thesis, Virginia Polytechnic Institute and State University, Blacksburg, Virginia 24061.
- , F.K. ROSS, and G.V. GIBBS (1977) An X-ray and neutron diffraction study of hydrous low cordierite. *Am. Mineral.* 62, 67-78.
- CURRIE, K.L. (1971) The reaction  $3 \text{ cordierite} = 2 \text{ garnet} + 4 \text{ sillimanite} + 5 \text{ quartz}$  as a geological thermometer in the Opinicon Lake region, Ontario. *Contr. Mineral. Petrol.* 33, 215-226.
- DESMARQUEST, L. (1965) Multilayer refractory coatings for the interior parts of internal combustion engines. French Patent 1,393,475.
- FARRELL, E.F., and R.E. NEWNHAM (1967) Electronic and vibrational absorption spectra in low cordierite. *Am. Mineral.* 52, 380-388.



- FESSLER, A.H. (1938) Cordierite compositions suitable for spark-plug insulators. U.S. Patent 2,106,598.
- FISCHER, G.R., D.L. EVANS, and J.E. GEIGER (1974) Crystal lattice thermal expansion of cordierite. (Abstr.) *Crystallographic Assoc. Progr. and Abstr. Series 2, 2*, 214; and personal communication (1977).
- GIBBS, G.V. (1966) The polymorphism of cordierite, I: The crystal structure of low cordierite. *Am. Mineral.* 51, 1068-1087.
- GOLDMAN, D.S., G.R. ROSSMAN, and W.A. DOLLASE (1977) Personal communication.
- GOSTELOW, C.R., and J.E. RESTALL (1972) Ceramic with potential gas-turbine application. *Proc. Brit. Ceram. Soc.* 22, 117-127.
- HAMILTON, W.C. (1965) Significance tests on the crystallographic R factor. *Acta Crystallogr.* 18, 502-510.
- HAZEN, R.M., and C.T. PREWITT (1977) Effects of temperature and pressure on interatomic distances in oxygen-based minerals. *Am. Mineral.* 62, 309-315.
- HENSEN, B.J., and D.H. GREEN (1971) Experimental study of the stability of cordierite and garnet in pelitic compositions at high pressures and temperatures. I. Compositions with excess alumino-silicate. *Contrib. Mineral. Petrol.* 33, 309-330.
- JOHNSON, C.K. (1965) ORTEP, a Fortran thermal ellipsoid plot program for crystal structure illustrations. U.S. Tech. Inf. Serv. *ORNL* 3794.
- KARKHANAVALA, M.D., and F.A. HUMMEL (1953) The polymorphism of cordierite. *J. Am. Ceram. Soc.* 36, 389-392.

- KHAN, A.A. (1976) Computer simulation of thermal expansion of non-cubic crystals: forsterite, anhydrite and scheelite. *Acta Crystallogr.* A32, 11-16.
- LACH, V. (1974) The occurrence of iron-cordierite in the black cores of stoneware pipes. *Interceram.* NR3, 214-218.
- LACHMAN, I.M., and R.M. LEWIS (1973) Anisotropic cordierite monolith. U.S. Patent 3,885,977.
- LANGER, K., and W. SCHREYER (1976) Apparent effects of molecular water on the lattice geometry of cordierite: A discussion. *Am. Mineral.* 61, 1036-1040.
- LEE, J.D., and J.L. PENTECOST (1976) Properties of flux-grown cordierite single crystals. *J. Am. Ceram. Soc.* 59, 183.
- LEVIEN, L., and J.J. PAPIKE (1976) Scapolite crystal chemistry: Aluminum-silicon distributions, carbonate group disorder, and thermal expansion. *Am. Mineral.* 61, 864-877.
- MAGNAN, R. (1971) Concrete of low thermal expansion. *Ger. Offen.* 2,063,386.
- MEAGHER, E.P. (1967) *The Crystal Structure and Polymorphism of Cordierite*. Ph.D. Dissertation, The Pennsylvania State University, University Park, Pennsylvania 16802.
- , and G.V. GIBBS (1966) Crystal structure and polymorphism of cordierite. (Abstr.) *Geol. Soc. Am. Spec. Pap.* 87, 107.
- , and ——— (1967) Tetrahedral magnesium in cordierite. (Abstr.) *Geol. Soc. Am. Ann. Mtg.*, New Orleans, 146.
- , and ——— (1977) The polymorphism of cordierite: II. The crystal structure of indialite. *Can. Mineral.* 15, 43-49.

- MEIER, W.M., and H. VILLIGER (1969) Die Methode der Abstandsverfeinerung zur Bestimmung der Atomkoordinaten idealisierter Gerüststrukturen. *Z. Kristallogr.* 129, 411-423.
- MIYASHIRO, A., T. IYAMA, M. YAMASAKI, and T. MIYASHIRO (1955) The polymorphism of cordierite and indialite. *Am. J. Sci.* 253, 185-208.
- NAGASAKI, S., Y. NISHIKAWA, N. OKAMOTO, and H. NAKAHARA (1970) Unfired and fired basic refractory linings. German Patent 1,802,337.
- NEWTON, R.C. (1972) An experimental determination of the high-pressure stability limits of magnesian cordierite under wet and dry conditions. *J. Geol.* 80, 398-420.
- PRYCE, M.W. (1973) Low-iron cordierite in phlogopite schist from White Well, Western Australia. *Mineral. Mag.* 39, 241-243.
- RATHGEBER, R., and H. FOWLER (1966) Iron-cordierite in the core structure of a bloated building brick. *J. Aust. Ceram. Soc.* 2(2), 52-53.
- RICHARDSON, H.M. (1949) Occurrence of iron-cordierite in blast furnace linings. *Mineral. Mag.* 28, 547-554.
- ROBINSON, P.D., and J.H. FANG (1977) Barylite,  $\text{BaBe}_2\text{Si}_2\text{O}_7$ : Its space group and crystal structure. *Am. Mineral.* 62, 167-169.
- SCHREYER, W., and J.F. SCHAIRER (1961) Compositions and structural states of anhydrous Mg-cordierite: A reinvestigation of the central part of the system  $\text{MgO}-\text{Al}_2\text{O}_3-\text{SiO}_2$ . *J. Petrol.* 2, 324-406.
- SKINNER, B.J. (1966) *Handbook of Physical Constants*. Geol. Soc. Am., pp. 76-96.

- SOEJIMA, S. (1974) High-strength ceramic honeycomb structure. *Japan. Kokai* 74 88, 908.
- STANEK, J., and J. MISKOVSKY (1964) Iron-rich cordierite from a pegmatite near Dolni Bory, W. Moravia, Czechoslovakia. *Casopis Mineral. Geol.* 9, 191-192.
- STOUT, J.H. (1976) Apparent effects of molecular water on the lattice geometry of cordierite: A reply. *Am. Mineral.* 61, 1041-1044.
- STRUNZ, H., C.H. TENNYSON, and P. UEBEL (1971) Cordierite. *Mineral. Sci. Eng.* 3, 3-18.
- SUENO, S., M. CAMERON, J.J. PAPIKE, and C.T. PREWITT (1973) The high temperature crystal chemistry of tremolite. *Am. Mineral.* 58, 649-664.
- TAKANE, K., and T. TAKEUCHI (1936) The crystal structure of cordierite. *Japan. Assoc. Mineral. Petrol. Econ. Geol. J.* 16, 101-127.
- TAKAO, H., K. TOGAWA, and K. MATOBA (1974) Heat-resistant, honey-combed layer. *Ger. Offen.* 2,337,034.
- TSANG, T., and S. GHOSE (1972) Nuclear magnetic resonance of  $^1\text{H}$  and  $^{27}\text{Al}$  and Al-Si order in low cordierite,  $\text{Mg}_2\text{Al}_4\text{Si}_5\text{O}_{18}\cdot n\text{H}_2\text{O}$ . *J. Chem. Phys.* 56, 3329-3332.

## APPENDIX A: THE PSEUDO-AXES OF CORDIERITE

### INTRODUCTION

Cordierite is pseudo-hexagonal and has two zones, [110] and [310], that look remarkably similar to [100] and [010], respectively. Hence, care is required in distinguishing these zones in single crystal photographs of the mineral.

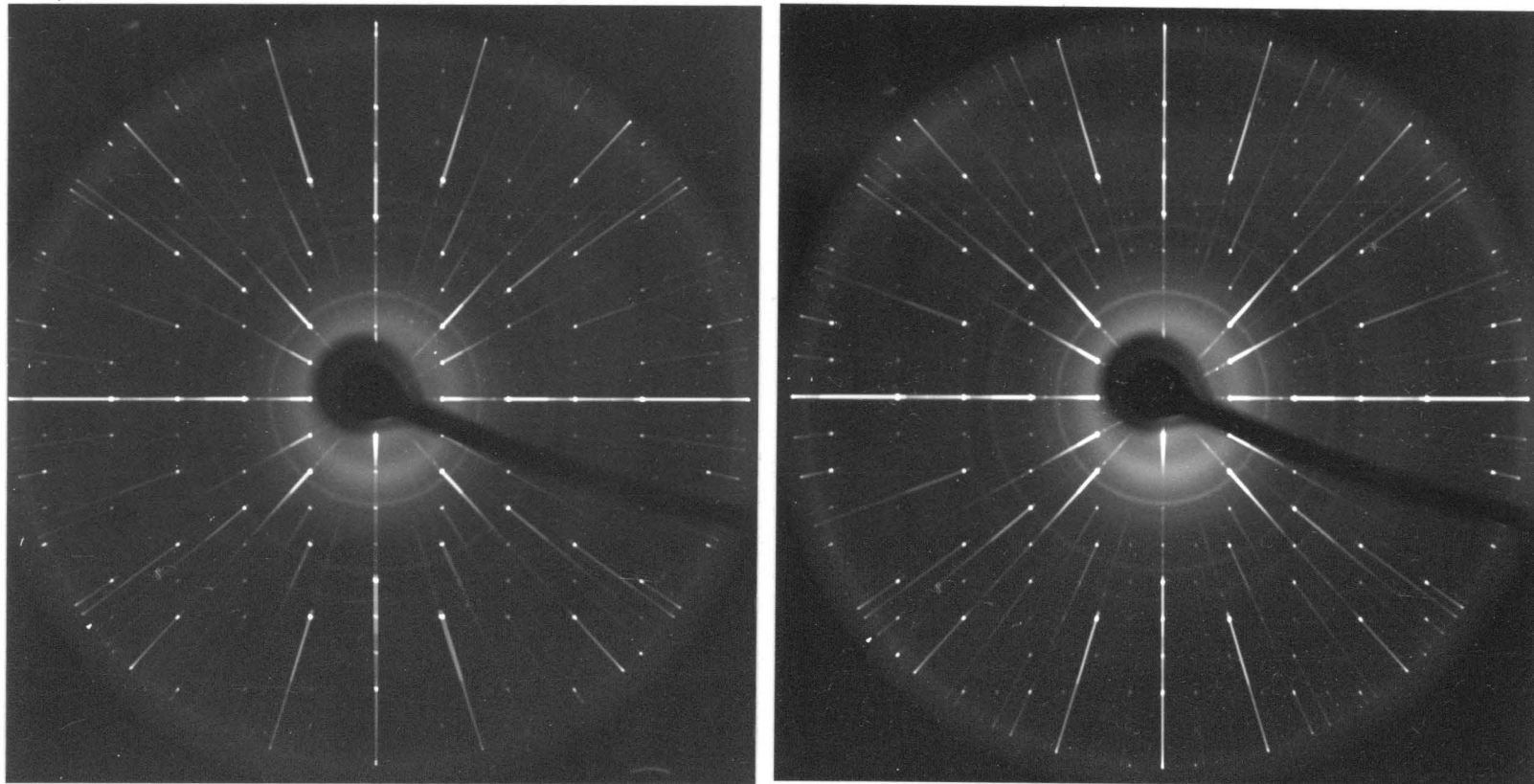
The first crystal structure determinations of cordierite were undertaken independently by Takane and Takeuchi (1936) and by Byström (1942). However, the results of these were slightly different and as Miyashiro *et al.* (1955) remarked, "Though all these investigations adopted the point group  $mmm$  ( $D_{2h}$ ) and the space group  $Ccmm$  ( $D_{2h}^{20}$ ) as a basis of their structure studies, Takane and Takeuchi state that they observed, under favorable conditions, very weak reflections incompatible with this space group - such as (401), (601), (801), (10•0•1)." This led later investigators to wonder whether the true space group was  $Ccmm$  or perhaps  $Cmmm$ , the latter being consistent with the extra reflections observed by Takane and Takeuchi. Gibbs (1966) showed that by orienting the crystal on its pseudo-axes, the indexed peaks of the type (h0ℓ, h even, ℓ odd) were indeed present, but when oriented on the true axes, no peaks of this type were recorded. The author has also observed peaks of the type (0kℓ, k even, ℓ odd) when mounted on the pseudo-axes which also violates  $Ccmm$ . But again, no such peaks are recorded when the crystal is oriented properly. Cohen (1975) has since confirmed the space group  $Ccmm$  for cordierite.

The purpose of this note is to show the hazards of accidentally orienting cordierite on its pseudo-axes and how easy it is to do so. Suggestions are also made on how to avoid this problem. The crystal used for the precession photographs was White Well cordierite,  $a = 17.09$ ,  $b = 9.73$ ,  $c = 9.36$ , and was the same one previously used for the high temperature data collection.

#### CALCULATIONS

In order to show how similar the pseudo-axes are to the true ones, the following calculations were made.

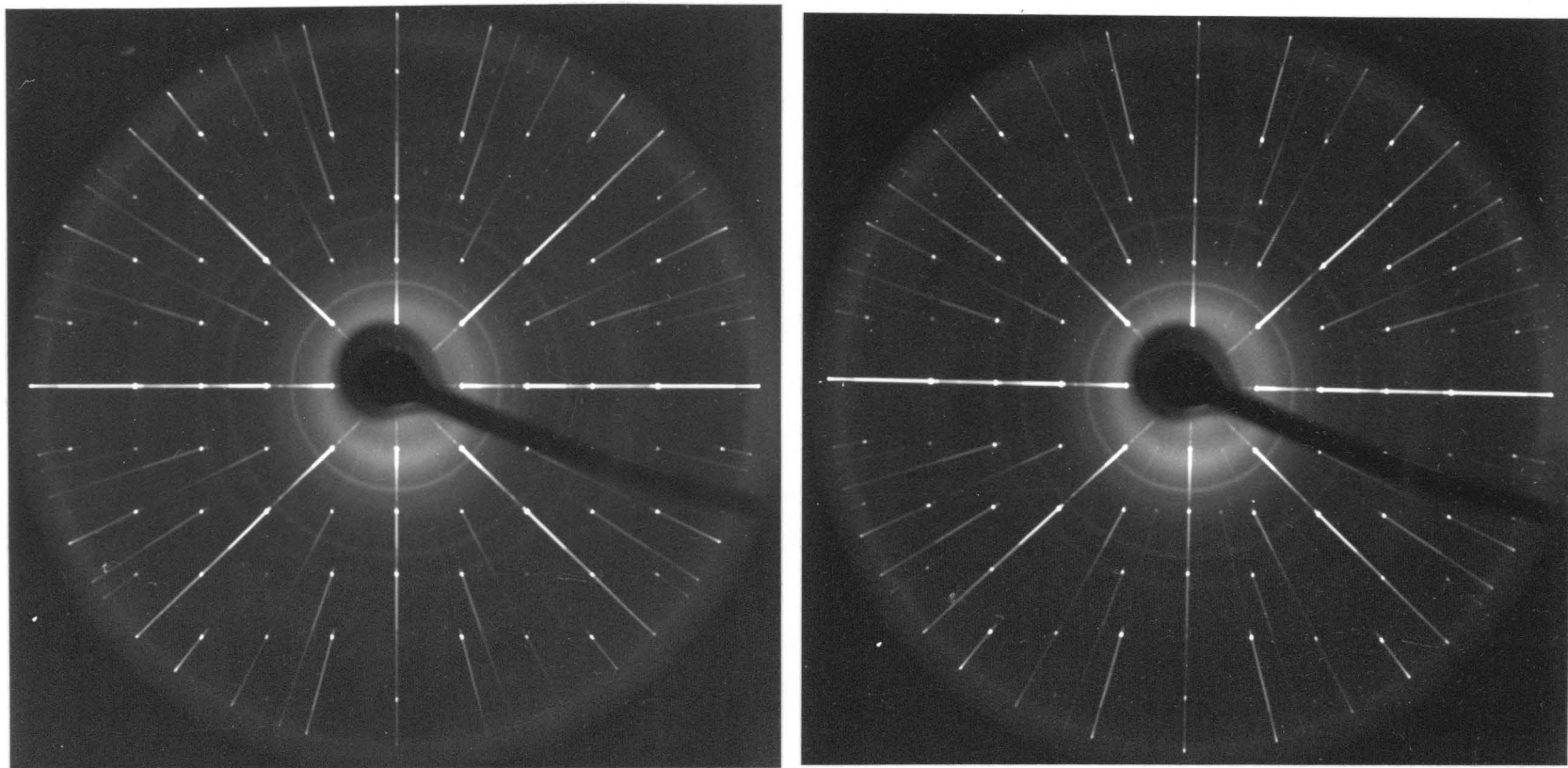
We know that  $x = F \cdot d^*$  where  $x$  is the distance in mm measured on the film along a zone,  $d^*$  is the spacing of reciprocal planes corresponding to  $x$ , and  $F$  is the crystal-to-film distance, which in our case is 60 mm. We also know that  $d^* = \lambda/p$ , where  $p$  is the period in the direct lattice. Combining these two equations, we have  $x = 60 \cdot \lambda/p$ . Now we can calculate the distance between peaks on a precession photograph. (Note: this equation does not take into account the possibility of systematic absences.) For  $a$  we have  $x = 60 \cdot 0.7107/17.08 = 2.50$  mm. Because of the condition  $h00$ ,  $h = 2n$  for *Cc*cm, we would expect the distance between the peaks in the  $a^*$  direction to be  $2x$  or 5.00 mm. For peaks on the  $[110]$  direction (pseudo- $a$ ), we must first find  $d(110)$ . We know that  $r^*(110) = 1/d(110)$  and that  $r^*(110) = a^* + b^*$ . Also,  $a^* = 1/a = 1/17.09 = 0.059$  and  $b^* = 1/b = 1/9.73 = 0.103$ . Then  $r^*(110) = (a^{*2} + b^{*2})^{1/2} = 0.12$  and  $d(110) = 8.45 \text{ \AA}$ . Therefore,  $x = 60 \cdot 0.7107/8.45 = 5.04$  mm. Since there are no systematic absences in this direction, the distance between peaks



(a)

(b)

Figure 1. Precession photographs of the White Well cordierite after heating. The dial axis for both is  $c^*$ . (a)  $a^*$  is the vertical axis and the dial setting is  $345^\circ$ . (b)  $[110]^*$  is the vertical axis and the dial setting is  $45^\circ$ . The powder rings in both photographs are from secondary hematite which formed during heating. (See main text.)



(a)

(b)

Figure 2. Precession photographs of the White Well cordierite after heating. The dial axis for both is  $c^*$ . (a)  $b^*$  is the vertical axis and the dial setting is  $75^\circ$ . (b)  $[310]^*$  is the vertical axis and the dial setting is  $15^\circ$ . The powder rings in both photographs are from secondary hematite which formed during heating. (See main text.)



on the film is 5.04 mm.

Similar calculations for  $b^*$  and  $[310]^*$  show that distances between peaks on a photograph for these two directions are 8.76 mm and 8.68 mm, respectively.

#### DISCUSSION

When measuring from the center, the difference between the spacing of peaks on the real and pseudo-axes for lower order reflections is indistinguishable on x-ray film. Only out at higher order reflections ( $n > 10$ ) can the differences start to be detected by simple ruler measurement. Figures 1 and 2 illustrate this point. The dial axis is  $c$  for all of these photographs. The precession photograph on the left of each figure shows the true axial direction as the vertical axis and the right has the pseudo-axis as the vertical axis. Dial settings are shown to give angular relationships. Note that all four photographs have Friedel symmetry  $mm2$ .

It is easy to see why picking  $[110]$  and  $[310]$  as axial directions is very easy unless caution is observed. This mistake leads to poor cell parameter measurements, peak intensity measurement errors, and indexed peaks that violate space group absences. Suggestions to avoid this dilemma are in order. (1) It is preferable to have  $c$  as the rotation axis of a precession or Weissenberg photograph. If this is the case,  $a$ ,  $b$ ,  $[110]$  and  $[310]$  are all in the same photograph and can be directly compared and axes properly assigned. (2) If the rotation axis is  $a$  or  $b$ , it is suggested to find the two candidates for either the  $a$  or  $b$  axis and directly

compare the two photographs. Thus one can be sure of the real and pseudo-directions without having to accurately measure cell parameters which are known to vary with cation substitution. (3) Use optical means for orienting the crystal. Bloss (1977) has excellent optical techniques for orienting single crystals.

APPENDIX B: INSTALLATION, CALIBRATION, AND OPERATING  
PROCEDURES FOR A SINGLE-CRYSTAL HEATER IN  
CONJUNCTION WITH A FOUR-CIRCLE DIFFRAC-  
TOMETER

INTRODUCTION

The single crystal heater used in the cordierite study was designed and described by Brown, Sueno, and Prewitt (1973). The heater is relatively simple and convenient to use in that its geometry allows data collection up to  $65^{\circ}2\theta$  and it is easily retracted for room temperature work. The maximum operating temperature of the heater is approximately  $1200^{\circ}\text{C}$ .

The purpose of this appendix is to review the procedure of furnace installation, specialized crystal mounting techniques, calibration procedures, and general operating procedures. A complete list of all essential starting materials and mailing addresses (when appropriate) of suppliers is also given.

INTEGRAL STARTING MATERIALS

- 1.\* Crystal heater
2. Power supply
3. Voltage stabilizer
4. Digital voltmeter (covering up to approximately 15 mV)
5. Chart recorder (1 mV, 5 mV, and 10 mV ranges, full scale)
6. Short collimators (allows positioning of kapton shield)
7. Power and thermocouple leads for wiring
8. Binocular microscope
9. Micrometer ocular
10. Crystal remounting device
11. Micro (small tip) soldering iron

---

\* Addresses are given for these items

12. Lakeside 70 resin
- 13.\* Zircoa bond 6 and  $ZrO_2$
14. Silica or mullite glass wool
15. Vacuum pump
16. Biological pipettes
- 17.\* Silica glass capillaries (0.3 and 0.5 mm sizes)
18. Silica glass fibers
19. Small tube furnace for curing cement
20. Small lab vise with teflon covered jaws
21. Small tip acetylene-oxygen torch
- 22.\* Pt and Pt-13% Rh thermocouple wire, 0.003", bare
23. Small diameter teflon tubing
24. Various compounds for melting point calibration
- 25.\* Kapton (1 mil thickness)

#### ADDRESSES OF SELECTED SUPPLIERS

1. Blake Industries, Inc.  
P.O. Box 464  
52 Commerce Street  
Springfield, N.J. 07081
13. Zirconium Corporation of America  
P.O. Box 39217  
Solon, Ohio 44139
17. Uni-Mex Co.  
1829 N. Arborgast Ave., 1-G  
Griffen, Indiana 46319
22. Omega Engineering, Inc.  
Box 4047  
Stamford, Conn. 06907
25. DuPont  
Station Plaza Building  
20 Evergreen Place  
East Orange, N.J. 07018

#### INSTALLATION

The furnace as manufactured by Blake Industries is shown in Figures 1 and 2. It is a resistance heater with two ceramic prongs containing coils of Pt.-10% Rh. wire. Care must be taken not to bend or crack this ceramic. The furnace itself has 4 wire leads.

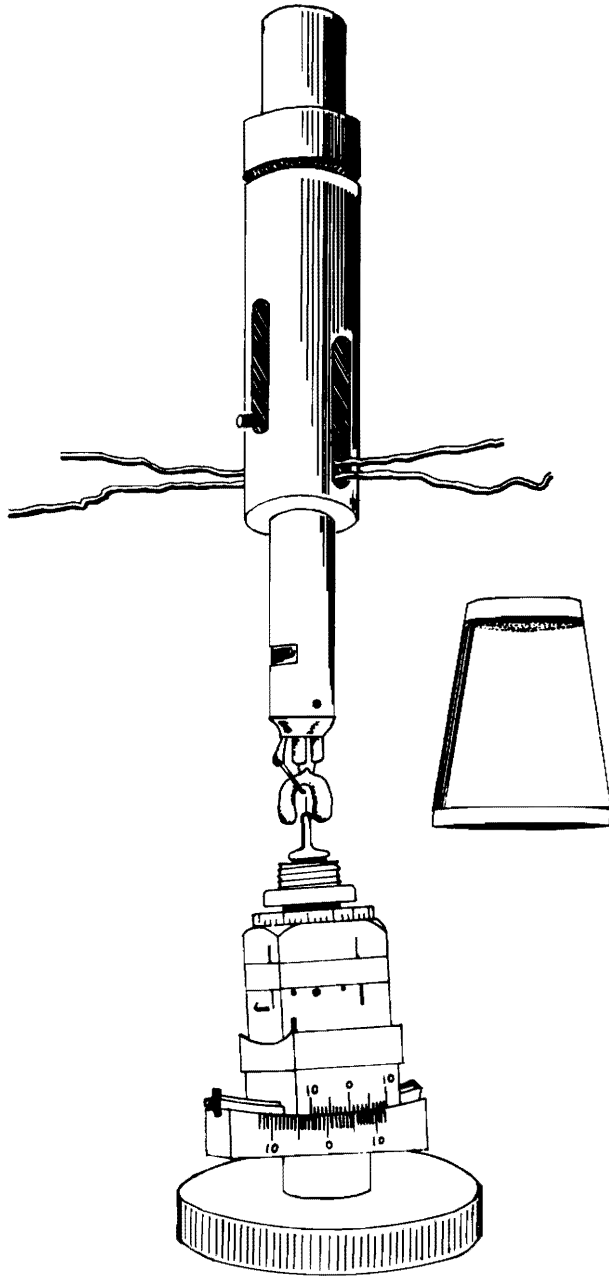


Figure 1. Single crystal heater with the aluminum post fully extended. The post can be retracted for room temperature data collection. The kapton shield, which covers the heater prongs and crystal to dampen temperature fluctuations, is shown on the right. (After Brown *et al.* (1973).)

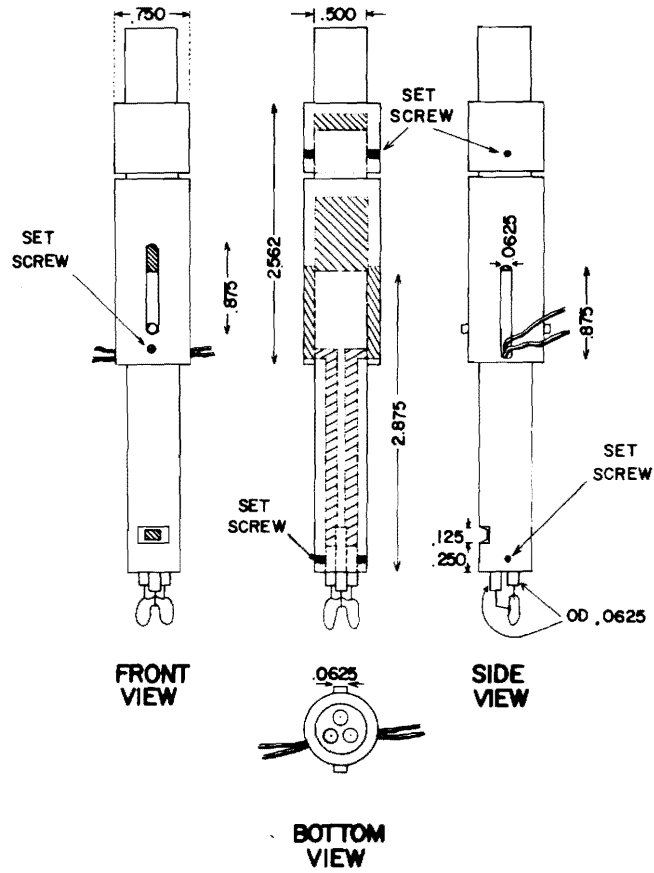


Figure 2. Plan view of the single crystal heater. (After Brown *et al.* (1973).)

The multi-strand wires are power leads whereas the single strand wires are Pt.-10% Rh. thermocouple leads. The heating element is mounted on an adjustable post that can be raised or lowered to the desired position. Because of this adjustable post, complete removal of the furnace is unnecessary for normal room temperature data collection. It is recommended that data collection be performed in the lower hemisphere dictating that the furnace be mounted "upside-down" in the upper hemisphere. The brass  $\chi$ -circle of the Picker FACS-I is already drilled to receive the end post of the furnace. A set screw will be needed to hold the end post of the furnace in its pre-drilled hole.

A typical power supply for this furnace is described in Brown *et al.* (1973). The setup in our laboratory utilizes a 50 watt, 15 amp maximum power source with a 120 volt constant voltage transformer for line current stabilization. A thermocouple feed-back control, if obtainable, would be outstanding for a constant temperature maintenance at various  $\chi$  settings. (See the operating procedures for more detail.)

Various wiring configurations have been used. Our setup is fairly simple and works quite well. All four leads from the furnace are run to one four-lead terminal that has been attached to the  $\chi$ -circle (about 5" from the furnace) on a homemade bracket. Four extension wires (single strand copper wire will do for the thermocouple wire extensions) are run from the other side of the terminal up to a fine gauge extension spring (attached to the top of the glass cage) and then out the nearest top corner of the glass cage. The spring is specially placed so that it can give and take slack from the four extension wires at any data collection position without allowing the

wires to touch the hot X-ray collimator. (X-ray collimators can get hot enough to melt wire insulation.) The terminal, then, serves the purpose of keeping the extensions from tugging unnecessarily on the wire connections within the furnace.

#### CRYSTAL MOUNTING TECHNIQUE

##### 1. Initial Mounting

- a. It is essential for high temperature work that the crystal is completely free of dirt, oil, and wax. It can usually be cleaned with a good acetone wash.
- b. Using a micro-soldering iron, melt a small amount of lakeside 70 on a glass fiber.
- c. Under the binocular microscope, bring the fiber up to the crystal and remelt the lakeside, attaching the crystal to the fiber. The cement should cover only a minimal area of the crystal; avoid coating the entire crystal with the cement.
- d. Mount the fiber on a goniometer head and align the crystal in the normal manner with a precession camera. For crystals that are mounted randomly, the Bloss spindle stage technique is an easy method for alignment (Bloss, 1977).

##### 2. Remounting Crystal for High Temperature Work

- a. Place the goniometer head with aligned crystal on a crystal remounting device. Be sure to have the crystal in position so it can be remounted on a



desired crystallographic direction.

- b. Make a careful sketch of the crystal at stage settings of  $0^\circ$  and  $90^\circ$  and indicate the dimensions of the crystal.
- c. Place a 3 to 4 cm long silica glass fiber mounted in clay on another goniometer head and place it on the opposite end of the remounting device.
- d. The high temperature cement must now be mixed. The first step is to grind either silica glass wool or mullite wool as fine as possible (this takes 3-5 minutes with a large mortar and pestle) wetting the wool with acetone before grinding. Dry the resulting powder. Place a very small amount on a glass slide and add a few drops of Zircoa Bond 6 and mix to a soupy consistency. The cement dries quickly and more Zircoa can be added to keep the cement from stiffening.
- e. Using a needle or thin probe, place a small amount of the cement on the end of the long free fiber and immediately run the fiber tip up to the crystal.
- f. Again, the amount of cement used is critical. If too little cement is used, the higher temperatures may affect the mount. More cement may be added with a needle. If too much cement is used,

a later mounting step may be impossible. Excess cement may be removed by coating a needle with a film of Zircoa and dissolving away the unwanted portion.

- g. Let dry for about an hour. A drawing of the mounting procedure to this stage is shown in Figure 3.
- h. Using the micro-soldering iron, melt the lakeside 70 on the original mount and retract that fiber. The crystal is now mounted in high temperature cement with a desired crystallographic direction approximately in line with the quartz fiber.
- i. Carefully break the fiber away from the goniometer head and place it into either a 0.3 or 0.5 mm capillary, depending on the size of your mount. Let the crystal and fiber slide down to the end of the capillary.<sup>1</sup> The crystal should rest approximately 0.5 mm from the inner end of the glass capillary. Cement to this capillary a larger biological pipette with a good coating of Duco cement as shown in Figure 4a.
- j. When the Duco is dry, place the large end of the pipette in a small table vise with teflon covered

---

<sup>1</sup> If the crystal gets stuck along the way, an appropriate size fiber may be put down the capillary to gently shove the end of the fiber with mounted crystal farther along.

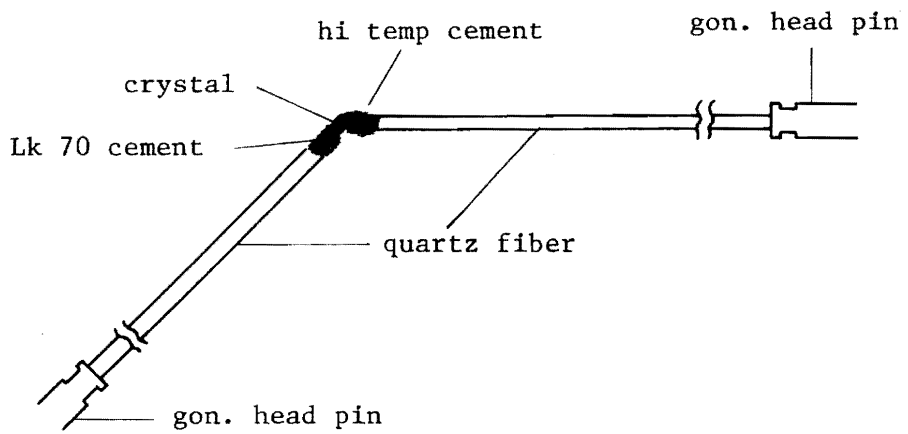


Figure 3. Remounting the crystal in high temperature cement along a known zone. The quartz fiber that the crystal is remounted on must be at least 3 to 4 cm long.

jaws and attach a vacuum hose to the pipette.

- k. While the capillary is being evacuated, place it in a small tube furnace (or the equivalent) capable of 90-100°C and cure the cement in this temperature range for at least two hours (overnight if possible). This will properly prepare the cement for surviving extreme temperatures.
- l. At this point make sure the crystal is still on the fiber and that the crystal is approximately 0.5 mm away from the inner end of the tube. Light taps on the vise may be used to position the crystal with attached fiber.<sup>2</sup> Also, the crystal should be no more than 1 mm away from the outer end of the capillary.
- m. Next, using a small tip oxygen-acetylene torch, cut through the capillary at a point near the end of the quartz fiber. The result is shown in Figure 4b.
- n. Finally, mix some fast drying epoxy and mount the evacuated tube in a brass goniometer head pin. Leave about 1.5 cm of the tube exposed. (Make sure you have the correct end of the capillary sticking out!) As a safeguard, it is usually advisable for the user

---

<sup>2</sup> However, this is sometimes unsuccessful and it is best to position the crystal properly when it is initially slid down the capillary.

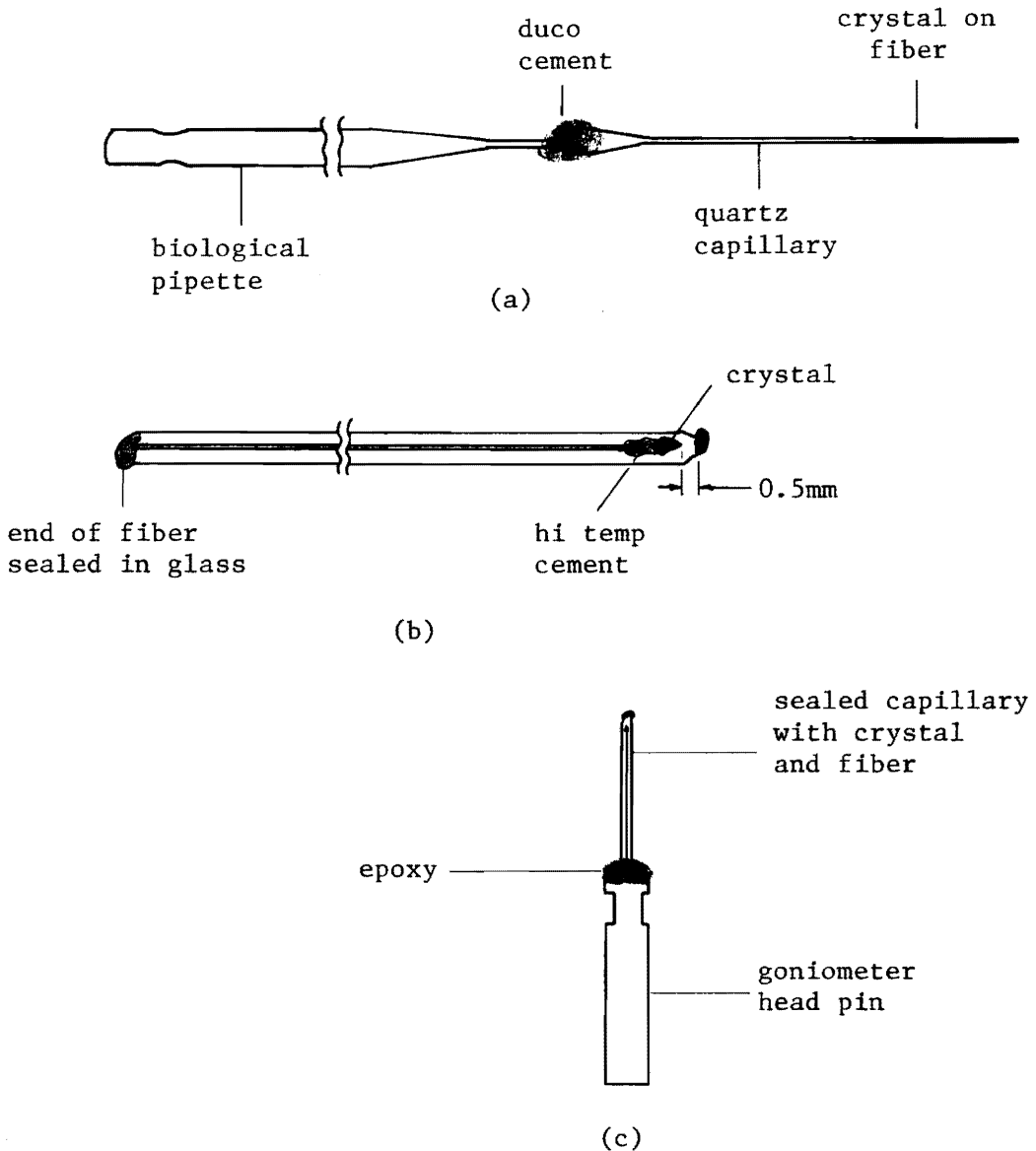


Figure 4. (a) Pipette, capillary configuration just before the vacuum hose is attached to the pipette. (b) Evacuated and sealed glass capillary. Note the distance from the crystal to the inner end of the capillary and that the quartz fiber is embedded in the opposite inner end. (c) The final product. The epoxy may be coated with high temperature cement so it will not soften during data collection at high temperatures.

to coat the dried epoxy with high temperature cement. The final mounting procedure is shown in Figure 4c.

NOTE: This mounting procedure is by far the most difficult procedure of the entire operation. Each step is essential and has a high potential for failure even when extreme care is taken. Patience and practice and a little luck are required.

#### FURNACE CALIBRATION

The furnace is calibrated using two independent methods. Even though only one method will provide the actual calibration curve for the furnace, the other also provides valuable information.

##### 1. Calibration Thermocouple Method

- a. Figure 5 shows the calibration thermocouple and all its component parts. The setup is mounted in a copper pin which is attached to a goniometer head.
- b. The actual measuring technique involves monitoring both the calibration thermocouple and the permanent furnace thermocouple simultaneously. A switch can be rigged to permit a single voltmeter to be connected to either thermocouple depending on its position.
- c. Attach the goniometer head with calibrating thermocouple to the four-circle and center the connecting bead in the cross hairs of the telescope.

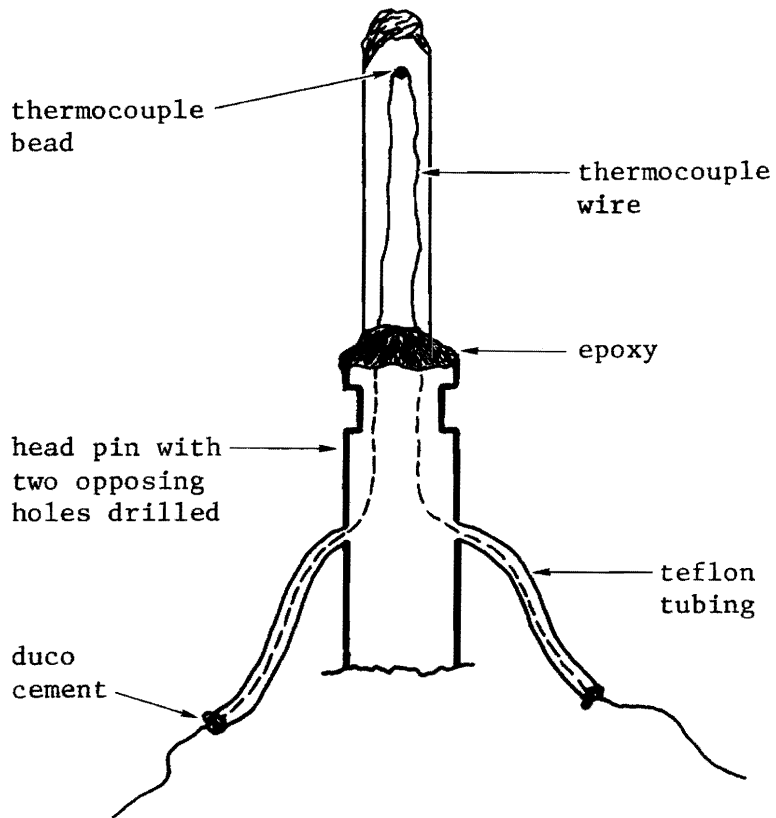


Figure 5. The calibration thermocouple shown mounted within a head pin and quartz capillary.

- d. Adjust the furnace into its fully extended position.

If the furnace is adjusted correctly, the calibrating thermocouple bead should be symmetrically between the two heater prongs and the measuring and calibration thermocouples should be separated by approximately 1 to 2 mm. If necessary, the furnace position can be adjusted slightly by carefully bending the supporting rods to the heater prongs.

- e. The position that the bead of the calibration thermocouple has now assumed should be very close to the furnace hot spot. To check this, heat the furnace up to several hundred degrees (see operating instructions) and set  $\chi = 0^\circ$ . After the temperature is stable, adjust the goniometer sledges and Z-translation until the highest temperature reading is obtained. If the starting position of the bead (step (c) above) is not the hot spot of the furnace, the furnace position must again be adjusted. Correct configuration is reached when the heater is fully extended and the thermocouple bead is centered in the cross hairs and also in the furnace hot spot.

- f. Adjust the temperature of the furnace until the measuring thermocouple reads approximately  $200^\circ\text{C}$ . Make sure the furnace temperature is stabilized by waiting several minutes. Make a chart to record the  $\chi$  setting, the calibration and furnace thermocouple readings in mV, and



the temperature at the calibration thermocouple tip.<sup>3</sup>

Collect readings at  $\chi$  settings of  $0^\circ$ ,  $45^\circ$  and  $90^\circ$ .

Notice that the temperature changes slightly with  $\chi$  setting. This will be discussed later.

- g. Repeat this procedure at approximately  $400^\circ\text{C}$ ,  $600^\circ\text{C}$ ,  $800^\circ\text{C}$  and  $900^\circ\text{C}$ .
- h. Plot the furnace thermocouple mV readings *vs* temperature measured by the calibration thermocouple for a  $\chi$  setting of  $0^\circ$ .

## 2. Crystal Melting Point Calibration

- a. This method involves melting crystals with known melting points in the furnace. The procedure will provide the actual calibration curve for the furnace which will be used during experimental runs. The shape of this curve will be the approximate shape of the thermocouple curve, but this curve will be lower on the plot and accurate to an absolute degree. The calibration thermocouple acts as a heat sink of low thermal mass and thus is not solely accurate.

The melting point samples we used are shown in Table 1 along with their melting temperatures.

---

<sup>3</sup> Remember that when using thermocouple mV-temperature equivalence charts, the cold junction is usually  $0^\circ\text{C}$ . mV readings must be corrected for room temperature data collection.

TABLE 1

## Melting Point Crystals

Compound	Melting temperature*
Benzoic Acid	123°C
D-camphor	186-188°C
Anthracene	216°C
NaNO <sub>3</sub>	307°C
B <sub>2</sub> O <sub>3</sub>	460°C
KIO <sub>3</sub>	560°C
Ba(NO <sub>3</sub> ) <sub>2</sub>	592°C
KCl	776°C
NaCl	801°C
BaCl <sub>2</sub>	962°C

---

\* Note that there is not a crystal listed that melts around 700°C. Any appropriate substance can be used if so desired to obtain data at this temperature.

- b. Under a binocular microscope, pick an appropriate melting point crystal. The largest dimension should be no greater than 0.4 mm and the crystal must possess sharp (not rounded) corners.
- c. Since crystal alignment is not relevant here, the crystal can be mounted arbitrarily with high temperature cement.
- d. The crystal is put in a capillary, evacuated, *etc.*, exactly like the experimental crystal. This is to assure that the melting point crystal melts under the same conditions as the experimental crystal.
- e. With the melting point crystal in the hot spot of the furnace and  $\chi$  set to  $0^\circ$ , raise the furnace temperature very slowly while constantly watching the crystal through the telescope. The melting point mV value should be predicted beforehand from the thermocouple curve so that the observer can anticipate melting. Remember that the thermocouple curve will predict slightly higher mV readings at melting than will actually be observed.
- f. Melting begins when the crystal edges start to round, and the voltmeter reading should be recorded at this point. Once a crystal is melted it should not be used again. Even if part of the crystal is still intact, its corners are rounded rendering it useless.

- g. Plot temperature *vs* mV readings at each melting point. This is the final plot and the furnace is now calibrated (see Fig. 6).

#### FURNACE OPERATING PROCEDURE

##### 1. Recalibrating the Furnace

There are only two reasons for the furnace to ever be in need of recalibration. First, if the ceramic coating of the platinum heating coils cracks badly enough for platinum vapor to leak at high temperature or to cause a change in the hot spot, the furnace may have to be rebuilt and recalibrated. Second, any other catastrophe which brings damage to other parts of the furnace may slightly change its characteristics and it again will be in need of recalibration.

##### 2. General Operation

- a. A schematic sketch of the entire setup is shown in Figure 7.
- b. Always keep the kapton film in place when collecting data. This greatly restricts temperature variation.
- c. It is necessary for the power supply to have a coarse and a fine adjustment. Also, an AC current stabilizer interconnected with the power supply is needed to dampen power, and thus temperature, fluctuations.
- d. A strip chart recorder is necessary to keep track of the temperature changes during data collection when

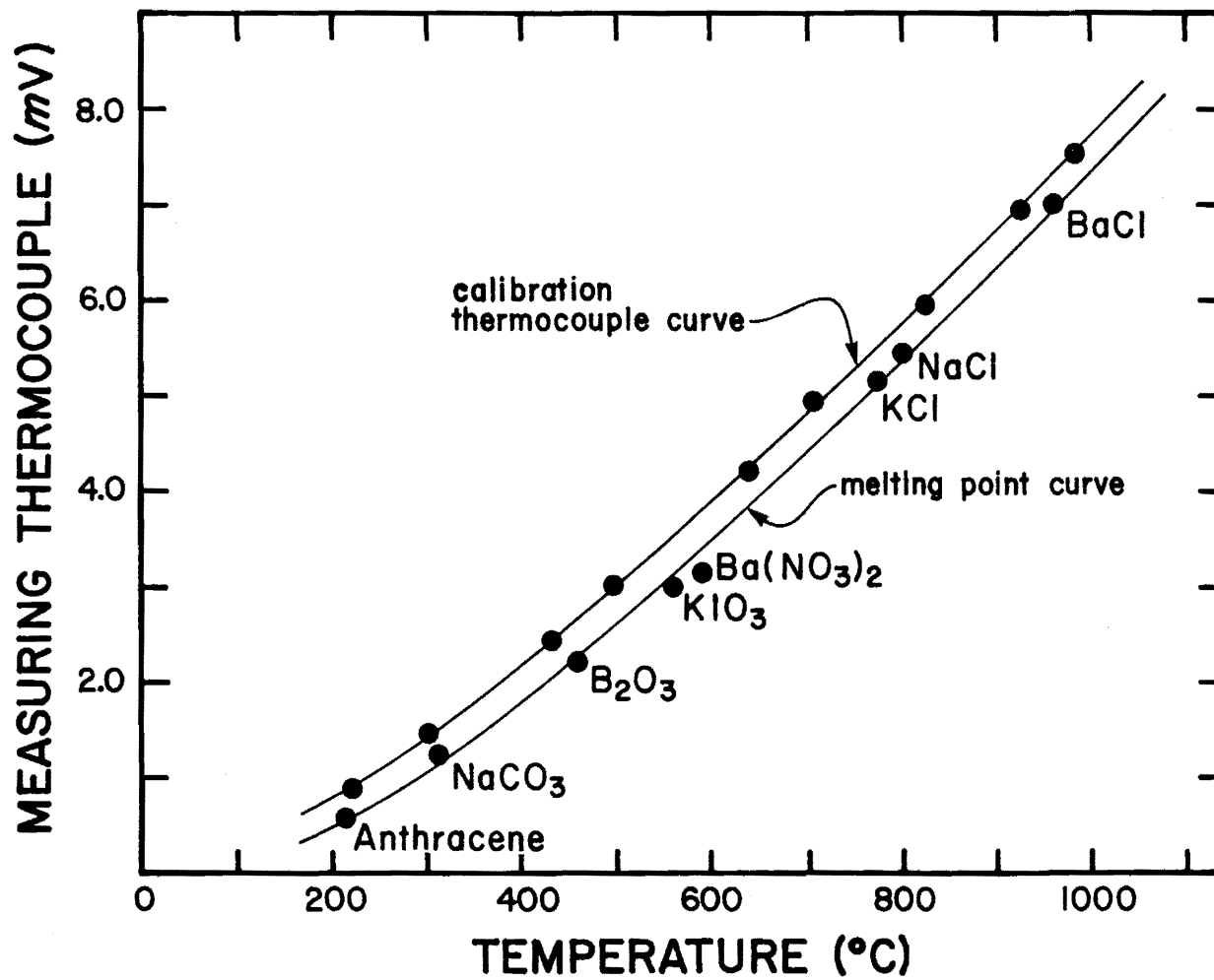


Figure 6. The final callibration plot for our furnace. This plot varies slightly from furnace to furnace.

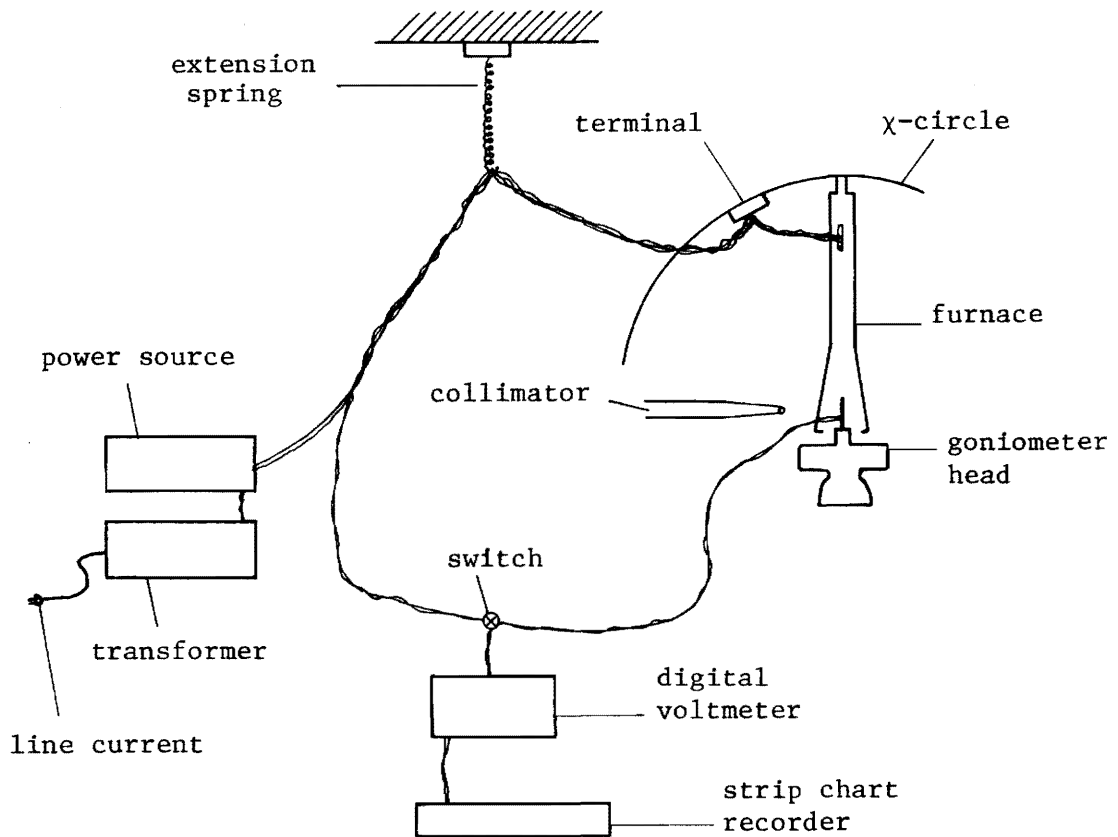


Figure 7. Schematic diagram of our high temperature data collecting setup.

the observer is not present.

- e. When the furnace has been set at a certain temperature, it is a good idea to let the crystal equilibrate at this temperature for at least 12 hours. Also check for temperature fluctuation at this time.
- f. Never raise the furnace temperature above 1200°C and to be completely safe, 1000°C. At temperatures above 1200°C the platinum heating coils start to vaporize.
- g. Due to the configuration of the kapton shield and heat convection, there is a change in furnace temperature simply with a change in  $\chi$ . The temperature change ranges from  $\pm 5^\circ$  at low temperatures to as much as  $\pm 20^\circ$  at 1000°C, depending on the position of  $\chi$  between  $0^\circ$  and  $90^\circ$ . If these temperature changes cannot be tolerated, a thermocouple feedback controller may be installed.
- h. After much testing, it has been shown that one should not attempt to collect data at a  $2\theta$  greater than  $65^\circ$ . At this point, the prongs start to interfere with diffracted radiation and will significantly affect the weaker reflections.
- i. It is extremely advantageous and almost necessary to keep the goniometer head in the lower hemisphere and the heater in the upper hemisphere during data collection. This keeps the heat trapped within the shield and away from the goniometer head which could

show alignment deviations with temperature change.

- j. As an alternative to (g) above, the  $\chi$  temperature dependence can be removed by collecting data within small ranges ( $10^\circ - 20^\circ$ ) of  $\chi$ . The heater current can be adjusted for each segment of data collection to maintain a constant crystal temperature.



APPENDIX C: OBSERVED (FO) AND CALCULATED (FC) STRUCTURAL  
AMPLITUDES FOR THE WHITE WELL AND DOLNI BORY  
CORDIERITES AT VARIOUS TEMPERATURES



TABLE C-1, continued.

Table with 16 columns (L, FO, FC, L, FO, FC, L, FO, FC, L, FO, FC, L, FO, FC, L, FO, FC) and multiple rows of numerical data. The table is organized into groups of rows, each starting with a header row (e.g., 'H= 9 K= 11') and followed by several rows of data. The data values are integers, some positive and some negative, representing various measurements or counts. The table is dense and contains a large volume of data points.









TABLE C-4. Structural Amplitudes for the Dolni Bory Cordierite at 24°C (Ccm).

Table with multiple columns (L, FO, FC) and rows of numerical data representing structural amplitudes for Dolni Bory Cordierite. Each row corresponds to a specific reflection and includes associated Miller indices (hkl) and intensity values.



TABLE C-4, continued.

Table with multiple columns of numerical data and headers (L, FO, FC) repeated across the top. The data is organized into rows, with some rows containing labels like 'H=13 K=5' or 'H=17 K=15'.











APPENDIX D: FINAL FRACTIONAL COORDINATES AND THERMAL  
PARAMETERS FOR THE WHITE WELL AND DOLNI  
BORY CORDIERITES

Final fractional coordinates and thermal parameters ( $\times 10^5$ )  
for White Well cordierite at various temperatures

Atom	24°C*	375°C	775°C	24°C**	
T <sub>1</sub> 1(Al)	x	1/4	1/4	1/4	1/4
	y	1/4	1/4	1/4	1/4
	z	0.2502(1)	0.2500(2)	0.2500(2)	0.2502(1)
	$\beta_{11}$	57(3)	93(4)	126(6)	51(3)
	$\beta_{22}$	133(8)	224(12)	363(19)	106(10)
	$\beta_{33}$	110(9)	272(14)	429(22)	174(12)
	$\beta_{12}$	15(3)	22(5)	35(8)	15(4)
	$\beta_{13}$	0	0	0	0
	$\beta_{23}$	0	0	0	0
	B <sub>eq</sub> ***	0.52	0.96	1.46	0.54
T <sub>1</sub> 6(Si)	x	0	0	0	0
	y	1/2	1/2	1/2	1/2
	z	1/4	1/4	1/4	1/4
	$\beta_{11}$	39(3)	60(5)	88(7)	33(4)
	$\beta_{22}$	146(10)	245(15)	352(22)	170(12)
	$\beta_{33}$	98(10)	228(17)	342(25)	136(15)
	$\beta_{12}$	0	0	0	0
	$\beta_{13}$	0	0	0	0
	$\beta_{23}$	0	0	0	0
	B <sub>eq</sub>	0.45	0.81	1.19	0.50
T <sub>2</sub> 1(Si)	x	0.1926(1)	0.1920(1)	0.1917(1)	0.1924(1)
	y	0.0778(1)	0.0783(1)	0.0785(2)	0.0778(1)
	z	0	0	0	0
	$\beta_{11}$	38(2)	60(4)	87(5)	32(3)
	$\beta_{22}$	83(7)	155(11)	240(15)	91(9)
	$\beta_{33}$	118(8)	239(11)	373(20)	167(12)
	$\beta_{12}$	7(3)	11(5)	13(7)	1(4)
	$\beta_{13}$	0	0	0	0
	$\beta_{23}$	0	0	0	0
	B <sub>eq</sub>	0.39	0.71	1.08	0.44

\* All 24°C data from Cohen *et al.* (1977)

\*\* After heating

\*\*\* B<sub>eq</sub> is the isotropic equivalent of the anisotropic temperature factors calculated using the expression

$$B_{eq} = 4/3[\beta_{11}a^2 + \beta_{22}b^2 + \beta_{33}c^2 + 2\beta_{12}abc\cos\gamma + 2\beta_{23}bcc\cos\alpha + 2\beta_{13}acc\cos\beta]$$



Atom	24°C	375°C	775°C	24°C	
T <sub>2</sub> <sup>6</sup> (Al)	x	0.0508(1)	0.0506(1)	0.0500(1)	0.0508(1)
	y	0.3079(1)	0.3076(1)	0.3070(2)	0.3079(1)
	z	0	0	0	0
	β <sub>11</sub>	31(3)	62(4)	91(6)	32(3)
	β <sub>22</sub>	121(8)	220(12)	335(18)	124(10)
	β <sub>33</sub>	132(9)	268(15)	382(22)	153(13)
	β <sub>12</sub>	8(3)	21(5)	27(8)	5(4)
	β <sub>13</sub>	0	0	0	0
	β <sub>23</sub>	0	0	0	0
B <sub>eq</sub>	0.43	0.83	1.23	0.46	
T <sub>2</sub> <sup>3</sup> (Si)	x	-0.1352(1)	-0.1351(1)	-0.1347(1)	-0.1352(1)
	y	0.2375(1)	0.2369(1)	0.2363(2)	0.2374(1)
	z	0	0	0	0
	β <sub>11</sub>	37(2)	57(4)	86(5)	28(3)
	β <sub>22</sub>	99(7)	176(11)	273(16)	133(9)
	β <sub>33</sub>	105(8)	247(13)	340(19)	141(11)
	β <sub>12</sub>	-11(3)	-14(4)	-40(7)	-13(4)
	β <sub>13</sub>	0	0	0	0
	β <sub>23</sub>	0	0	0	0
B <sub>eq</sub>	0.39	0.73	1.08	0.44	
O <sub>1</sub> <sup>1</sup>	x	0.2474(1)	0.2470(1)	0.2468(2)	0.2473(1)
	y	0.1029(1)	0.1036(2)	0.1042(3)	0.1034(2)
	z	0.1410(2)	0.1407(3)	0.1398(4)	0.1409(2)
	β <sub>11</sub>	74(5)	137(7)	217(12)	66(5)
	β <sub>22</sub>	153(13)	277(22)	414(36)	282(16)
	β <sub>33</sub>	179(15)	308(25)	450(38)	153(20)
	β <sub>12</sub>	9(5)	24(9)	16(16)	3(8)
	β <sub>13</sub>	-31(6)	-40(11)	-122(19)	-31(8)
	β <sub>23</sub>	-19(11)	-68(19)	-95(29)	-11(16)
B <sub>eq</sub>	0.69	1.25	1.90	0.79	
O <sub>1</sub> <sup>6</sup>	x	0.0620(1)	0.0620(1)	0.0619(2)	0.0623(1)
	y	0.4160(2)	0.4166(2)	0.4159(3)	0.4166(2)
	z	0.1512(2)	0.1512(3)	0.1510(4)	0.1513(2)
	β <sub>11</sub>	54(5)	90(7)	122(10)	57(5)
	β <sub>22</sub>	211(13)	376(21)	550(33)	215(17)
	β <sub>33</sub>	180(15)	331(25)	545(39)	198(21)
	β <sub>12</sub>	17(6)	24(10)	23(16)	-3(8)
	β <sub>13</sub>	-2(6)	-16(11)	-73(17)	10(8)
	β <sub>23</sub>	-71(11)	-150(19)	-234(32)	-72(15)
B <sub>eq</sub>	0.69	1.21	1.81	0.73	

Atom	24°C	375°C	775°C	24°C	
O <sub>1</sub> <sup>3</sup>	x	-0.1732(1)	-0.1736(1)	-0.1734(2)	-0.1733(1)
	y	0.3101(2)	0.3090(2)	0.3082(4)	0.3102(2)
	z	0.1416(2)	0.1418(3)	0.1422(4)	0.1414(2)
	β <sub>11</sub>	54(4)	111(7)	179(12)	60(5)
	β <sub>22</sub>	202(14)	342(22)	501(35)	174(17)
	β <sub>33</sub>	199(15)	285(25)	549(42)	209(21)
	β <sub>12</sub>	-11(6)	-26(10)	-55(17)	-20(8)
	β <sub>13</sub>	20(6)	36(10)	95(18)	21(8)
	β <sub>23</sub>	-29(11)	-90(19)	-140(32)	-39(15)
	B <sub>eq</sub>	0.70	1.20	1.98	0.70
O <sub>2</sub> <sup>1</sup>	x	0.1223(1)	0.1220(2)	0.1216(3)	0.1222(2)
	y	0.1839(2)	0.1846(4)	0.1843(6)	0.1844(3)
	z	0	0	0	0
	β <sub>11</sub>	70(7)	135(12)	165(18)	73(8)
	β <sub>22</sub>	248(21)	368(35)	615(59)	178(25)
	β <sub>33</sub>	386(25)	718(50)	1206(94)	401(36)
	β <sub>12</sub>	51(9)	133(16)	217(27)	61(12)
	β <sub>13</sub>	0	0	0	0
	β <sub>23</sub>	0	0	0	0
	B <sub>eq</sub>	1.04	1.83	2.83	0.98
O <sub>2</sub> <sup>6</sup>	x	-0.0430(1)	-0.0434(2)	-0.0438(3)	-0.0432(2)
	y	0.2476(2)	0.2478(4)	0.2484(6)	0.2487(3)
	z	0	0	0	0
	β <sub>11</sub>	53(7)	69(11)	122(17)	58(8)
	β <sub>22</sub>	301(21)	594(39)	883(69)	261(25)
	β <sub>33</sub>	330(24)	711(49)	875(76)	360(34)
	β <sub>12</sub>	-27(9)	-31(15)	-14(26)	-33(12)
	β <sub>13</sub>	0	0	0	0
	β <sub>23</sub>	0	0	0	0
	B <sub>eq</sub>	0.97	1.85	2.62	0.98
O <sub>2</sub> <sup>3</sup>	x	-0.1645(1)	-0.1641(2)	-0.1630(3)	-0.1646(2)
	y	0.0792(2)	0.0793(3)	0.0778(5)	0.0803(3)
	z	0	0	0	0
	β <sub>11</sub>	91(7)	163(12)	243(20)	88(8)
	β <sub>22</sub>	144(19)	189(30)	298(45)	140(25)
	β <sub>33</sub>	361(23)	779(50)	850(70)	412(35)
	β <sub>12</sub>	-37(9)	-76(15)	-155(25)	-2(12)
	β <sub>13</sub>	0	0	0	0
	β <sub>23</sub>	0	0	0	0
	B <sub>eq</sub>	0.96	1.79	2.32	1.00

Atom	24°C	375°C	775°C	24°C
x	0.1625(1)	0.1622(1)	0.1626(1)	0.1624(1)
y	1/2	1/2	1/2	1/2
z	1/4	1/4	1/4	1/4
$\beta_{11}$	48(3)	75(4)	109(7)	44(3)
$\beta_{22}$	142(9)	259(14)	385(20)	122(11)
$\beta_{33}$	181(9)	436(16)	655(26)	225(13)
$\beta_{12}$	0	0	0	0
$\beta_{13}$	0	0	0	0
$\beta_{23}$	0(7)	8(12)	30(20)	5(10)
$B_{eq}$	0.58	1.13	1.68	0.59

Final fractional coordinates and thermal parameters ( $\times 10^5$ )  
for Dolni Bory cordierite at two temperatures

Atom	24°C ( <i>Ccsm</i> )	24°C ( <i>Ccc2</i> )	375°C	
$T_1^{1Al}$	x	1/4	1/4	1/4
	y	1/4	1/4	1/4
	z	0.2502(3)	0.2494(5)	0.2501(4)
	$\beta_{11}$	41(6)	71(13)	94(9)
	$\beta_{22}$	104(15)	129(29)	208(28)
	$\beta_{33}$	64(15)	64(32)	140(26)
	$\beta_{12}$	14(7)	29(14)	38(12)
	$\beta_{13}$	0	0	0
	$\beta_{23}$	0	0	0
	$B_{eq}^*$	0.37		0.80
$T_1^{1_iAl}$	x	-	3/4	-
	y	-	3/4	-
	z	-	0.7493(5)	-
	$\beta_{11}$	-	18(11)	-
	$\beta_{22}$	-	72(26)	-
	$\beta_{33}$	-	72(31)	-
	$\beta_{12}$	-	-2(12)	-
	$\beta_{13}$	-	0	-
$T_1^{6Si}$	x	0	0	0
	y	1/2	1/2	1/2
	z	1/4	0.2486	1/4
	$\beta_{11}$	31(8)	32(8)	17(10)
	$\beta_{22}$	122(20)	114(18)	219(34)
	$\beta_{33}$	44(20)	53(26)	144(35)
	$\beta_{12}$	0	0	0
	$\beta_{13}$	0	0	0
	$\beta_{23}$	0	0	0
	$B_{eq}$	0.33		0.52

\*  $B_{eq}$  is the isotropic equivalent of the anisotropic temperature factors calculated using the expression

$$B_{eq} = 4/3[\beta_{11}a^2 + \beta_{22}b^2 + \beta_{33}c^2 + 2\beta_{12}ab\cos\gamma + 2\beta_{23}bcc\cos\alpha + 2\beta_{13}acc\cos\beta].$$

Atom	24°C ( <i>Cccm</i> )	24°C ( <i>Ccc2</i> )	375°C	
T <sub>2</sub> 1Si	x	0.1901(1)	0.1900(1)	0.1895(2)
	y	0.0794(2)	0.0792(2)	0.0795(3)
	z	0	0	0
	β <sub>11</sub>	37(6)	38(6)	65(9)
	β <sub>22</sub>	38(14)	61(14)	144(25)
	β <sub>33</sub>	64(17)	57(17)	117(29)
	β <sub>12</sub>	12(7)	12(7)	4(12)
	β <sub>13</sub>	0	0	0
	β <sub>23</sub>	0	0	0
B <sub>eq</sub>	0.31		0.58	
T <sub>2</sub> 6Al	x	0.0501(1)	0.0501(1)	0.0499(2)
	y	0.3076(2)	0.3081(2)	0.3077(3)
	z	0	-0.0013(8)	0
	β <sub>11</sub>	33(7)	30(7)	43(9)
	β <sub>22</sub>	64(16)	85(16)	162(28)
	β <sub>33</sub>	69(19)	97(22)	208(32)
	β <sub>12</sub>	13(8)	7(8)	39(13)
	β <sub>13</sub>	0	-62(27)	0
	β <sub>23</sub>	0	-113(38)	0
B <sub>eq</sub>	0.29		0.62	
T <sub>2</sub> 3Si	x	-0.1347(1)	-0.1347(1)	-0.1350(2)
	y	0.2343(2)	0.2343(2)	0.2344(3)
	z	0	-0.0023(8)	0
	β <sub>11</sub>	34(7)	33(6)	59(9)
	β <sub>22</sub>	43(15)	62(14)	151(26)
	β <sub>33</sub>	73(16)	68(19)	140(28)
	β <sub>12</sub>	-22(7)	-23(7)	-12(12)
	β <sub>13</sub>	0	-45(22)	0
	β <sub>23</sub>	0	78(30)	0
B <sub>eq</sub>	0.28		0.59	
O <sub>1</sub>	x	0.2442(2)	0.2447(4)	0.2438(3)
	y	0.1052(3)	0.1053(0)	0.1049(5)
	z	0.1415(3)	0.1418(6)	0.1412(5)
	β <sub>11</sub>	69(12)	89(23)	101(16)
	β <sub>22</sub>	129(27)	217(56)	296(52)
	β <sub>33</sub>	93(28)	102(54)	269(56)
	β <sub>12</sub>	-15(14)	-36(27)	18(23)
	β <sub>13</sub>	-44(16)	-106(32)	-80(26)
	β <sub>23</sub>	-34(24)	-86(46)	-40(44)
B <sub>eq</sub>	0.55		1.10	

Atom	24°C ( <i>Ccm</i> )	24°C ( <i>Ccc2</i> )	375°C	
O <sub>1</sub> <sup>1-i</sup>	x	-	0.7558(4)	-
	y	-	0.8948(6)	-
	x	-	0.8589(6)	-
	β <sub>11</sub>	-	50(21)	-
	β <sub>22</sub>	-	107(48)	-
	β <sub>33</sub>	-	162(55)	-
	β <sub>12</sub>	-	2(24)	-
	β <sub>13</sub>	-	13(30)	-
	β <sub>23</sub>	-	48(43)	-
O <sub>1</sub> <sup>6</sup>	x	0.0611(2)	0.0607(4)	0.0609(3)
	y	0.4144(4)	0.4145(7)	0.4151(5)
	z	0.1522(4)	0.1513(7)	0.1509(5)
	β <sub>11</sub>	70(12)	90(24)	95(15)
	β <sub>22</sub>	207(29)	310(61)	324(48)
	β <sub>33</sub>	134(33)	107(59)	285(60)
	β <sub>12</sub>	30(14)	64(29)	23(23)
	β <sub>13</sub>	23(16)	49(31)	-18(25)
	β <sub>23</sub>	-58(26)	-114(50)	-131(46)
B <sub>eq</sub>	0.69		1.13	
O <sub>1</sub> <sup>6-i</sup>	x	-	0.9387(4)	-
	y	-	0.5850(6)	-
	z	-	0.8469(7)	-
	β <sub>11</sub>	-	49(21)	-
	β <sub>22</sub>	-	144(48)	-
	β <sub>33</sub>	-	195(61)	-
	β <sub>12</sub>	-	9(24)	-
	β <sub>13</sub>	-	19(29)	-
	β <sub>23</sub>	-	33(46)	-
O <sub>1</sub> <sup>3</sup>	x	-0.1729(2)	-0.1723(4)	-0.1729(3)
	y	0.3053(4)	0.3054(7)	0.3049(5)
	z	0.1428(4)	0.1429(7)	0.1427(5)
	β <sub>11</sub>	80(13)	131(27)	65(17)
	β <sub>22</sub>	186(30)	272(61)	454(56)
	β <sub>33</sub>	94(30)	14(53)	254(60)
	β <sub>12</sub>	-21(14)	-46(28)	-45(23)
	β <sub>13</sub>	3(15)	1(29)	46(22)
	β <sub>23</sub>	-84(25)	-143(48)	-25(49)
B <sub>eq</sub>	0.67		1.14	

Atom	24°C ( <i>Cccm</i> )	24°C ( <i>Ccc2</i> )	375°C	
O <sub>1</sub> <sup>3</sup> <sub>1</sub>	x	-	0.1738(4)	-
	y	-	0.6942(6)	-
	z	-	0.8572(7)	-
	β <sub>11</sub>	-	27(21)	-
	β <sub>22</sub>	-	155(51)	-
	β <sub>33</sub>	-	160(58)	-
	β <sub>12</sub>	-	5(23)	-
	β <sub>13</sub>	-	11(26)	-
	β <sub>23</sub>	-	-16(45)	-
O <sub>2</sub> <sup>1</sup>	x	0.1188(3)	0.1189(3)	0.1200(5)
	y	0.1822(6)	0.1829(6)	0.1833(8)
	z	0	0.0019(18)	0
	β <sub>11</sub>	72(20)	66(19)	137(27)
	β <sub>22</sub>	176(45)	282(51)	270(78)
	β <sub>33</sub>	404(64)	373(68)	702(109)
	β <sub>12</sub>	66(20)	100(25)	109(38)
	β <sub>13</sub>	0	9(69)	0
	β <sub>23</sub>	0	374(92)	0
B <sub>eq</sub>	0.97		1.71	
O <sub>2</sub> <sup>6</sup>	x	-0.0435(4)	-0.0433(4)	-0.0434(4)
	y	0.2449(6)	0.2461(6)	0.2462(9)
	z	0	0.0026(19)	0
	β <sub>11</sub>	40(20)	54(20)	56(25)
	β <sub>22</sub>	363(56)	357(54)	579(94)
	β <sub>33</sub>	494(66)	543(79)	607(101)
	β <sub>12</sub>	-16(25)	-24(26)	-107(38)
	β <sub>13</sub>	0	-261(62)	0
	β <sub>23</sub>	0	-49(125)	0
B <sub>eq</sub>	1.20		1.67	
O <sub>2</sub> <sup>3</sup>	x	-0.1615(4)	-0.1618(4)	-0.1607(5)
	y	0.0778(5)	0.0780(5)	0.0766(7)
	z	0	-0.0016(15)	0
	β <sub>11</sub>	90(19)	127(21)	190(29)
	β <sub>22</sub>	101(40)	112(40)	115(70)
	β <sub>33</sub>	382(59)	462(74)	621(104)
	β <sub>12</sub>	7(22)	-8(23)	-69(35)
	β <sub>13</sub>	0	330(56)	0
	β <sub>23</sub>	0	-53(78)	0
B <sub>eq</sub>	0.93		1.62	

Atom	24°C ( <i>Ccsm</i> )	24°C ( <i>Cce2</i> )	375°C	
M	x	0.1632(1)	0.1631(1)	0.1632(1)
	y	1/2	0.5054(3)	1/2
	z	1/4	0.2546(5)	1/4
	$\beta_{11}$	47(4)	48(3)	80(5)
	$\beta_{22}$	119(8)	49(9)	256(15)
	$\beta_{33}$	162(9)	130(9)	402(18)
	$\beta_{12}$	0	-22(9)	0
	$\beta_{13}$	0	25(11)	0
	$\beta_{23}$	12(10)	-94(11)	11(17)
	B <sub>eq</sub>	0.53		1.11
NaCaFe	x	0	0	0
	y	0	0	0
	z	0	0	0
	B	3.5399(.84)	4.1322(.46)	4.8595(1.22)



APPENDIX E: INTERATOMIC DISTANCES AND ANGLES FOR THE  
WHITE WELL AND DOLNI BORY CORDIERITES AT  
VARIOUS TEMPERATURES

$T$ -O and O-O interatomic distances (Å) and O- $T$ -O angles (°) for the five tetrahedral sites *vs* temperature in White Well cordierite

		24°C	375°C	775°C	775°C* (DLS)	24°C**
$T_1 1-O_1 1$	[2]	1.760(2)	1.756(2)	1.758(3)	1.755	1.758(2)
$-O_1 3'$	[2]	1.757(2)	1.751(2)	1.751(3)	1.762	1.761(2)
Mean		1.758(1)	1.753(1)	1.754(2)	1.759	1.759(1)
$O_1 3''-O_1 3'$	[1]	2.873(3)	2.856(4)	2.862(7)	2.870	2.877(3)
$O_1 1-O_1 3''$	[2]	2.587(2)	2.591(3)	2.600(5)	2.601	2.591(2)
$-O_1 3'$	[2]	3.132(2)	3.119(3)	3.116(5)	3.125	3.134(3)
$-O_1 1'$	[1]	2.864(3)	2.875(5)	2.895(7)	2.863	2.859(4)
Mean		2.862(1)	2.859(2)	2.865(2)	2.864	2.864(1)
$O_1 3''-T_1 1-O_1 3'$	[1]	109.6(1)	109.3(2)	109.6(3)	109.0	109.6(1)
$O_1 1-T_1 1-O_1 3''$	[2]	94.7(1)	95.3(1)	95.6(2)	95.3	94.8(1)
$-O_1 3'$	[2]	125.9(1)	124.6(1)	125.2(2)	125.4	125.9(1)
$-O_1 1'$	[1]	109.0(1)	108.7(2)	108.2(2)	109.3	108.8(2)
Mean		110.0(1)	110.0(1)	109.9(1)	109.9	110.0(1)
$T_1 6-O_1 6$	[4]	1.626(2)	1.625(2)	1.631(3)	1.626	1.628(2)
Mean		1.626(2)	1.625(2)	1.631(3)	1.626	1.628(2)
$O_1 6-O_1 6'$	[2]	2.813(3)	2.815(5)	2.819(7)	2.828	2.821(4)
$-O_1 6'''$	[2]	2.676(3)	2.673(4)	2.684(6)	2.677	2.681(4)
$-O_1 6''$	[2]	2.467(3)	2.463(5)	2.475(6)	2.470	2.462(4)
Mean		2.652(1)	2.650(2)	2.659(2)	2.658	2.655(2)
$O_1 6-T_1 6-O_1 6'$	[2]	119.7(1)	120.0(2)	119.6(3)	119.5	120.0(1)
$-O_1 6'''$	[2]	110.7(1)	110.6(2)	110.7(3)	110.8	110.8(1)
$-O_1 6''$	[2]	98.7(1)	98.5(2)	98.7(2)	98.8	98.2(1)
Mean		109.7(1)	109.7(1)	109.7(1)	109.7	109.7(1)

\* Simulated expansion by DLS. See text.

\*\* After heating.

		24°C	375°C	775°C	775°C* (DLS)	24°C**
$T_2 1-0_1 1$	[2]	1.636(2)	1.638(3)	1.633(3)	1.637	1.638(2)
$-0_2 3'$	[1]	1.601(2)	1.607(3)	1.603(5)	1.602	1.613(3)
$-0_2 1$	[1]	1.583(2)	1.584(3)	1.585(5)	1.584	1.589(3)
Mean		1.614(1)	1.617(2)	1.614(2)	1.615	1.619(1)
$O_1 1-0_1 1m$	[1]	2.638(3)	2.633(5)	2.616(7)	2.626	2.638(4)
$-0_2 1$	[2]	2.632(2)	2.634(4)	2.634(6)	2.637	2.636(3)
$-0_2 3'$	[2]	2.624(2)	2.631(4)	2.633(5)	2.629	2.636(3)
$O_2 1-0_2 3'$	[1]	2.659(3)	2.670(5)	2.654(7)	2.661	2.679(4)
Mean		2.635(1)	2.639(2)	2.634(2)	2.637	2.644(1)
$O_1 1-T_2 1-0_1 1m$	[1]	107.4(1)	107.0(2)	106.4(3)	106.6	107.3(1)
$-0_2 1$	[2]	109.7(1)	109.7(1)	109.8(2)	109.9	109.5(1)
$-0_2 3'$	[2]	108.3(1)	108.4(1)	108.9(2)	108.5	108.3(1)
$O_2 1-T_2 1-0_2 3'$	[1]	113.3(1)	113.3(1)	113.2(2)	113.3	113.6(1)
Mean		109.4(1)	109.4(1)	109.5(1)	109.5	109.4(1)
$T_2 3-0_1 3$	[2]	1.634(2)	1.640(3)	1.644(4)	1.638	1.637(2)
$-0_2 3$	[1]	1.619(2)	1.614(3)	1.622(5)	1.620	1.613(3)
$-0_2 6$	[1]	1.578(2)	1.574(3)	1.563(5)	1.580	1.577(3)
Mean		1.617(1)	1.617(2)	1.618(2)	1.619	1.616(1)
$O_1 3-0_1 3m$	[1]	2.649(3)	2.654(5)	2.660(7)	2.645	2.647(4)
$-0_2 6$	[2]	2.659(2)	2.662(4)	2.655(6)	2.663	2.658(3)
$-0_2 3$	[2]	2.613(2)	2.607(4)	2.619(6)	2.617	2.607(3)
$O_2 6-0_2 3$	[1]	2.644(3)	2.640(5)	2.636(7)	2.647	2.648(4)
Mean		2.640(1)	2.639(2)	2.641(2)	2.643	2.638(1)
$O_1 3-T_2 3-0_1 3m$	[1]	108.2(1)	108.0(2)	108.0(3)	107.9	107.9(2)
$-0_2 6$	[2]	111.6(1)	111.8(1)	111.8(2)	111.7	111.6(1)
$-0_2 3$	[2]	106.8(1)	106.5(1)	106.6(2)	106.8	106.7(1)
$O_2 6-T_2 3-0_2 3$	[1]	111.5(1)	111.8(1)	111.7(1)	111.6	111.6(1)
Mean		109.4(1)	109.4(1)	109.4(1)	109.4	109.4(1)

		24°C	375°C	775°C	775°C* (DLS)	24°C**
T <sub>2</sub> 6-O <sub>1</sub> 6	[2]	1.773(2)	1.779(3)	1.779(4)	1.775	1.779(2)
-O <sub>2</sub> 1	[1]	1.716(2)	1.711(3)	1.715(5)	1.717	1.715(3)
-O <sub>2</sub> 6	[1]	1.706(2)	1.710(3)	1.707(5)	1.707	1.710(3)
Mean		1.742(1)	1.745(1)	1.746(2)	1.744	1.746(1)
O <sub>1</sub> 6-O <sub>1</sub> 6m	[1]	2.829(3)	2.829(5)	2.824(7)	2.828	2.821(4)
-O <sub>2</sub> 6	[2]	2.812(2)	2.819(4)	2.820(6)	2.814	2.818(3)
-O <sub>2</sub> 1	[2]	2.856(2)	2.857(4)	2.855(5)	2.858	2.860(3)
O <sub>2</sub> 1-O <sub>2</sub> 6	[1]	2.890(3)	2.896(5)	2.904(7)	2.895	2.901(4)
Mean		2.842(1)	2.846(2)	2.846(2)	2.845	2.846(1)
O <sub>1</sub> 6-T <sub>2</sub> 6-O <sub>1</sub> 6m	[1]	105.8(1)	105.3(2)	105.0(3)	105.6	105.5(1)
-O <sub>2</sub> 6	[2]	107.8(1)	107.8(1)	108.0(2)	107.8	107.7(1)
-O <sub>2</sub> 1	[2]	109.9(1)	109.8(1)	109.6(2)	109.8	109.8(1)
O <sub>2</sub> 1-T <sub>2</sub> 6-O <sub>2</sub> 6	[1]	115.2(1)	115.7(1)	116.1(1)	115.5	115.7(1)
Mean		109.4(1)	109.4(1)	109.4(1)	109.4	109.4(1)

## Cation separation (Å) in White Well cordierite

		24°C	375°C	775°C	775°C* (DLS)	24°C**
<u>Six-membered ring</u>						
T <sub>2</sub> 1-T <sub>2</sub> 6	[2]	3.298(2)	3.293(2)	3.298(3)	3.300	3.302(2)
T <sub>2</sub> 6-T <sub>2</sub> 3	[2]	3.250(2)	3.252(2)	3.242(3)	3.255	3.256(2)
T <sub>2</sub> 3-T <sub>2</sub> 1	[2]	3.220(2)	3.221(2)	3.224(2)	3.222	3.225(2)
Mean		3.256(1)	3.255(1)	3.255(1)	3.259	3.261(1)
<u>Four-membered ring</u>						
T <sub>2</sub> 1-T <sub>1</sub> 1	[2]	3.042(1)	3.043(1)	3.045(2)	3.038	3.045(1)
T <sub>2</sub> 6-T <sub>1</sub> 6	[2]	3.117(1)	3.120(1)	3.123(1)	3.120	3.121(1)
T <sub>2</sub> 3-T <sub>1</sub> 1	[2]	3.053(1)	3.059(2)	3.066(2)	3.069	3.058(1)
Mean		3.071(1)	3.074(1)	3.078(1)	3.076	3.075(1)
<u>d(M-T)</u>						
M-T <sub>1</sub> 1	[2]	2.855(1)	2.861(1)	2.864(1)	2.867	2.861(1)
M-T <sub>1</sub> 6	[1]	2.776(1)	2.776(1)	2.789(2)	2.782	2.780(1)
Mean		2.829(1)	2.833(1)	2.839(1)	2.839	2.834(1)

\* Simulated expansion by *DLS*. See text.

\*\* After heating.

T-O-T and T-O-M angles (°) vs temperature  
for White Well cordierite

		24°C	375°C	775°C	775°C* (DLS)	24°C**
T <sub>2</sub> 1-O <sub>2</sub> 1-T <sub>2</sub> 6	[2]	176.0(2)	176.3(3)	176.3(4)	176.3	176.3(2)
T <sub>2</sub> 1-O <sub>2</sub> 3-T <sub>2</sub> 3	[2]	179.5(2)	179.0(3)	179.5(4)	180.0	179.0(2)
T <sub>2</sub> 3-O <sub>2</sub> 6-T <sub>2</sub> 6	[2]	163.5(2)	164.3(3)	164.8(4)	164.0	164.3(2)
Mean		173.0(1)	173.2(1)	173.5(2)	173.4	173.2(1)
T <sub>2</sub> 1-O <sub>1</sub> 1-T <sub>1</sub> 1	[2]	127.2(1)	127.2(1)	127.7(2)	127.1	127.4(1)
T <sub>2</sub> 6-O <sub>1</sub> 6-T <sub>1</sub> 6	[2]	132.9(1)	132.8(1)	132.6(2)	132.9	132.6(1)
T <sub>2</sub> 3-O <sub>1</sub> 3-T <sub>1</sub> 1	[2]	128.2(1)	128.7(1)	129.1(2)	128.9	128.3(1)
Mean		129.4(1)	129.6(1)	129.8(1)	129.6	129.4(1)
T <sub>1</sub> 1-O <sub>1</sub> 1-M	[2]	94.9(1)	94.8(1)	94.6(2)	94.9	95.0(1)
T <sub>1</sub> 1-O <sub>1</sub> 3-M	[2]	94.6(1)	94.6(1)	94.5(2)	94.3	94.6(1)
T <sub>1</sub> 6-O <sub>1</sub> 6-M	[2]	95.0(1)	95.1(1)	95.0(2)	95.0	95.2(1)
T <sub>2</sub> 1-O <sub>1</sub> 1-M	[2]	137.7(1)	137.6(1)	137.6(2)	137.8	137.5(1)
T <sub>2</sub> 3-O <sub>1</sub> 3-M	[2]	137.1(1)	136.3(1)	136.2(2)	136.5	137.0(1)
T <sub>2</sub> 6-O <sub>1</sub> 6-M	[2]	131.9(1)	131.8(1)	132.0(2)	131.7	131.9(1)
Mean		115.3(1)	115.0(1)	115.0(1)	115.0	115.2(1)

---

\* Simulated expansion by *DLS*. See text.

\*\* After heating.

M-O and O-O interatomic distances (Å) and O-M-O angles (°)  
for the octahedral site in White Well cordierite

		24°C	375°C	775°C	775°C* (DLS)	24°C**
M <sub>1</sub> -O <sub>1</sub> 6	[2]	2.113(2)	2.111(2)	2.124(4)	2.120	2.110(2)
-O <sub>1</sub> 1'	[2]	2.100(2)	2.116(2)	2.124(4)	2.121	2.110(2)
-O <sub>1</sub> 3'	[2]	2.115(2)	2.127(2)	2.135(4)	2.132	2.119(2)
Mean		2.108(1)	2.119(1)	2.128(2)	2.124	2.112(1)
O <sub>1</sub> 6-O <sub>1</sub> 6''	[1]	2.467(3)	2.463(4)	2.475(7)	2.470	2.462(4)
-O <sub>1</sub> 3'	[2]	2.902(2)	2.916(3)	2.917(5)	2.918	2.907(3)
O <sub>1</sub> 6''-O <sub>1</sub> 3'	[2]	3.272(2)	3.287(3)	3.304(5)	3.299	3.273(3)
O <sub>1</sub> 1''-O <sub>1</sub> 6''	[2]	3.261(2)	3.275(3)	3.288(5)	3.289	3.268(3)
O <sub>1</sub> 3'-O <sub>1</sub> 1'	[2]	2.587(2)	2.591(3)	2.600(5)	2.601	2.591(3)
-O <sub>1</sub> 1''	[2]	3.155(2)	3.175(3)	3.196(5)	3.184	3.165(3)
O <sub>1</sub> 1'-O <sub>1</sub> 1''	[1]	2.858(3)	2.875(5)	2.895(7)	2.877	2.859(4)
Mean		2.973(1)	2.986(1)	2.998(2)	2.994	2.977(1)
O <sub>1</sub> 6-M-O <sub>1</sub> 6''	[1]	71.4(1)	71.3(1)	71.3(1)	71.3	71.4(1)
-O <sub>1</sub> 3'	[2]	86.7(1)	86.9(1)	86.5(1)	86.6	86.8(1)
O <sub>1</sub> 6''-M-O <sub>1</sub> 3'	[2]	101.4(1)	101.7(1)	101.7(1)	101.7	101.4(1)
O <sub>1</sub> 1''-M-O <sub>1</sub> 6''	[2]	101.4(1)	101.6(1)	101.4(1)	101.7	101.5(1)
O <sub>1</sub> 3'-M-O <sub>1</sub> 1'	[2]	75.7(1)	75.3(1)	75.3(1)	75.4	75.6(1)
-O <sub>1</sub> 1''	[2]	96.9(1)	96.9(1)	97.3(1)	97.0	96.9(1)
O <sub>1</sub> 1''-M-O <sub>1</sub> 1'	[1]	85.8(1)	85.6(1)	85.9(2)	85.4	85.7(1)
Mean		90.1(1)	90.1(1)	90.1(1)	90.1	90.1(1)

\* Simulated expansion by DLS. See text.

\*\* After heating.

T-O and O-O interatomic distances (Å) and O-T-O angles (°)  
for the five tetrahedral sites in Dolni Bory cordierite

		24°C	375°C
T <sub>1</sub> 1-O <sub>1</sub> 1	[2]	1.748(4)	1.756(5)
-O <sub>1</sub> 3'	[2]	1.748(4)	1.750(5)
Mean		1.748(2)	1.753(3)
O <sub>1</sub> 3"-O <sub>1</sub> 3'	[1]	2.870(7)	2.873(9)
O <sub>1</sub> 1-O <sub>1</sub> 3"	[2]	2.618(5)	2.631(7)
-O <sub>1</sub> 3'	[2]	3.070(5)	3.072(6)
-O <sub>1</sub> 1'	[1]	2.892(6)	2.898(9)
Mean		2.856(3)	2.863(3)
O <sub>1</sub> 3"-T <sub>1</sub> 1-O <sub>1</sub> 3'	[1]	110.4(3)	110.3(4)
O <sub>1</sub> 1-T <sub>1</sub> 1-O <sub>1</sub> 3"	[2]	96.9(2)	97.2(2)
-O <sub>1</sub> 3'	[2]	122.7(2)	122.4(2)
-O <sub>1</sub> 1'	[1]	109.3(2)	109.3(4)
Mean		109.8(1)	109.8(1)
T <sub>1</sub> 6-O <sub>1</sub> 6	[4]	1.627(4)	1.631(5)
Mean		1.627(2)	1.631(3)
O <sub>1</sub> 6-O <sub>1</sub> 6'	[2]	2.785(7)	2.801(9)
-O <sub>1</sub> 6'''	[2]	2.697(7)	2.687(9)
-O <sub>1</sub> 6''	[2]	2.487(7)	2.493(9)
Mean		2.656(3)	2.665(4)
O <sub>1</sub> 6-T <sub>1</sub> 6-O <sub>1</sub> 6'	[2]	117.6(3)	118.3(4)
-O <sub>1</sub> 6'''	[2]	111.9(3)	110.9(4)
-O <sub>1</sub> 6''	[2]	99.3(3)	99.7(3)
Mean		109.6(1)	109.6(2)
T <sub>2</sub> 1-O <sub>1</sub> 1	[2]	1.634(4)	1.636(5)
-O <sub>2</sub> 3'	[1]	1.623(6)	1.616(7)
-O <sub>2</sub> 1	[1]	1.591(5)	1.576(7)
Mean		1.621(3)	1.616(3)



		24°C	375°C
$O_1 1-O_1 1m$	[1]	2.637(6)	2.633(9)
$-O_2 1$	[2]	2.642(6)	2.626(8)
$-O_2 3'$	[2]	2.647(6)	2.655(9)
$O_2 1-O_2 3'$	[1]	2.661(7)	2.655(9)
Mean		2.683(3)	2.680(4)
$O_1 1-T_2 1-O_1 1m$	[1]	107.6(3)	107.2(4)
$-O_2 1$	[2]	110.0(2)	109.7(3)
$-O_2 3'$	[2]	108.7(2)	108.7(3)
$O_2 1-T_2 1-O_2 3'$	[1]	111.8(3)	112.5(4)
Mean		109.5(1)	109.4(2)
$T_2 3-O_1 3$	[2]	1.641(3)	1.638(5)
$-O_2 3$	[1]	1.607(6)	1.615(7)
$-O_2 6$	[1]	1.575(6)	1.586(7)
Mean		1.616(2)	1.619(3)
$O_1 3-O_1 3m$	[1]	2.660(7)	2.663(9)
$-O_2 6$	[2]	2.664(7)	2.665(8)
$-O_2 3$	[2]	2.612(6)	2.621(8)
$O_2 6-O_2 3$	[1]	2.615(8)	2.624(9)
Mean		2.638(3)	2.643(3)
$O_1 3-T_2 3-O_1 3m$	[1]	108.3(3)	108.8(4)
$-O_2 6$	[2]	111.9(2)	111.5(3)
$-O_2 3$	[2]	107.0(2)	107.4(3)
$O_2 6-T_2 3-O_2 3$	[1]	110.5(3)	110.2(5)
Mean		109.4(1)	109.5(2)
$T_2 6-O_1 6$	[2]	1.773(4)	1.771(5)
$-O_2 1$	[1]	1.711(6)	1.721(7)
$-O_2 6$	[1]	1.726(6)	1.721(7)
Mean		1.746(3)	1.746(3)

		24°C	375°C
$O_1^6-O_1^6m$	[1]	2.832(7)	2.817(9)
$-O_2^6$	[2]	2.835(6)	2.826(8)
$-O_2^1$	[2]	2.866(6)	2.869(8)
$O_2^1-O_2^6$	[1]	2.864(8)	2.887(9)
Mean		2.850(3)	2.849(3)
$O_1^6-T_2^6-O_1^6m$	[1]	105.9(3)	105.3(4)
$-O_2^6$	[2]	108.2(2)	108.1(3)
$-O_2^1$	[2]	110.6(2)	110.5(2)
$O_2^1-T_2^6-O_2^6$	[1]	112.9(3)	114.0(4)
Mean		109.4(1)	109.4(1)

T-O-T and T-O-M angles (°) vs temperature  
for Dolni Bory cordierite

		24°C	375°C
T <sub>2</sub> 1-O <sub>2</sub> 1-T <sub>2</sub> 6	[2]	173.3(4)	175.1(6)
T <sub>2</sub> 1-O <sub>2</sub> 3-T <sub>2</sub> 3	[2]	179.0(4)	178.0(6)
T <sub>2</sub> 3-O <sub>2</sub> 6-T <sub>2</sub> 6	[2]	162.9(4)	163.6(6)
Mean		171.7(2)	172.2(3)
T <sub>2</sub> 1-O <sub>1</sub> 1-T <sub>1</sub> 1	[2]	128.7(2)	128.7(3)
T <sub>2</sub> 6-O <sub>1</sub> 6-T <sub>1</sub> 6	[2]	133.2(2)	133.4(3)
T <sub>2</sub> 3-O <sub>1</sub> 3-T <sub>1</sub> 1	[2]	129.4(2)	129.5(3)
Mean		130.4(1)	130.5(1)
T <sub>1</sub> 1-O <sub>1</sub> 1-M	[2]	94.4(2)	94.1(2)
T <sub>1</sub> 1-O <sub>1</sub> 3-M	[2]	94.1(2)	93.9(2)
T <sub>1</sub> 6-O <sub>1</sub> 6-M	[2]	94.1(2)	94.9(2)
T <sub>2</sub> 1-O <sub>1</sub> 1-M	[2]	136.6(2)	136.9(3)
T <sub>2</sub> 3-O <sub>1</sub> 3-M	[2]	136.0(2)	136.0(3)
T <sub>2</sub> 6-O <sub>1</sub> 6-M	[2]	131.1(2)	131.2(3)
Mean		114.4(1)	114.5(1)

## Cation separation (Å) in Dolni Bory cordierite

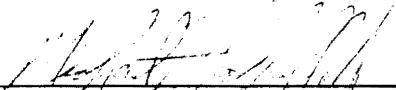
		24°C	375°C
<u>Six-membered ring</u>			
T <sub>2</sub> 1-T <sub>2</sub> 6	[2]	3.296(3)	3.294(4)
T <sub>2</sub> 6-T <sub>2</sub> 3	[2]	3.264(3)	3.294(4)
T <sub>2</sub> 3-T <sub>2</sub> 1	[2]	3.230(3)	3.231(4)
Mean		3.263(2)	3.273(2)
<u>Four-membered ring</u>			
T <sub>2</sub> 1-T <sub>1</sub> 1	[2]	3.052(2)	3.058(3)
T <sub>2</sub> 6-T <sub>1</sub> 6	[2]	3.123(2)	3.125(2)
T <sub>2</sub> 3-T <sub>1</sub> 1	[2]	3.064(3)	3.065(3)
Mean		3.080(1)	3.083(2)
<u>d(M-T)</u>			
M-T <sub>1</sub> 1	[2]	2.879(1)	2.881(1)
M-T <sub>1</sub> 6	[1]	2.812(1)	2.817(2)
Mean		2.857(1)	2.860(1)

M-O and O-O interatomic distances (Å) and  
O-M-O angles (°) for the octahedral site  
in Dolni Bory cordierite

		24°C	375°C
M <sub>1</sub> -O <sub>1</sub> 6	[2]	2.153(4)	2.161(5)
-O <sub>1</sub> 1'	[2]	2.154(4)	2.162(5)
-O <sub>1</sub> 3'	[2]	2.166(3)	2.173(5)
Mean		2.158(1)	2.165(3)
O <sub>1</sub> 6-O <sub>1</sub> 6''	[1]	2.482(7)	2.493(9)
-O <sub>1</sub> 3'	[2]	2.918(5)	2.936(7)
O <sub>1</sub> 6''-O <sub>1</sub> 3'	[2]	3.365(5)	3.368(7)
O <sub>1</sub> 1''-O <sub>1</sub> 6''	[2]	3.362(5)	3.377(6)
O <sub>1</sub> 3'-O <sub>1</sub> 1'	[2]	2.618(5)	2.631(6)
-O <sub>1</sub> 1''	[2]	3.277(5)	3.286(6)
O <sub>1</sub> 1'-O <sub>1</sub> 1''	[2]	2.856(6)	2.865(9)
Mean		3.035(2)	3.046(4)
O <sub>1</sub> 6-M-O <sub>1</sub> 6''	[1]	70.4(2)	70.4(3)
-O <sub>1</sub> 3'	[2]	85.0(1)	85.3(2)
O <sub>1</sub> 6''-M-O <sub>1</sub> 3'	[2]	102.4(1)	102.7(2)
O <sub>1</sub> 1''-M-O <sub>1</sub> 6''	[2]	102.7(1)	102.7(2)
O <sub>1</sub> 3'-M-O <sub>1</sub> 1'	[2]	74.6(1)	74.7(2)
-O <sub>1</sub> 1''	[2]	98.7(1)	98.6(2)
O <sub>1</sub> 1''-M-O <sub>1</sub> 1'	[1]	84.3(2)	84.2(3)
Mean		90.1(1)	90.2(1)

VITA

Michael Frederick Hochella, Jr. was born September 29, 1953 in Yokohama, Japan. He received a Bachelor of Science degree from Virginia Polytechnic Institute and State University in 1975.



---

Michael F. Hochella, Jr.

HIGH TEMPERATURE CRYSTAL CHEMISTRY OF HYDROUS  
Mg- and Fe-RICH CORDIERITES

by

Michael F. Hochella, Jr.

(ABSTRACT)

Structural refinements have been completed using data recorded for a Mg-rich cordierite at 24°C, 375°C, 775°C and 24°C (after heating to 775°C) and for an Fe-rich cordierite at 24°C and 375°C. The mean T-O bond lengths in both cordierites remain unchanged but the mean octahedral bonds (M-O) lengthen upon heating. The unusually low thermal expansion of the Mg-cordierite is the result of its relatively "rigid" tetrahedral framework and the anisotropic expansion of octahedra isolated from each other. This anisotropic expansion leads to a slight rotation of the six-membered rings, a concomitant collapse of the structure parallel to  $c$ , and an expansion parallel to  $a$  and  $b$ . In the Fe-cordierite, the Fe-octahedron is more flattened, resulting in  $c$  being smaller and  $a$  and  $b$  being larger than the cell dimensions in the Mg-cordierite. Upon heating Fe-cordierite, there is no evidence for a rotation of the rings and  $a$ ,  $b$  and  $c$  increase as the M-O bonds expand.

A re-examination of the water orientation in the cavities of the Mg-cordierite using neutron and X-ray  $\Delta\rho$  maps confirms the orientation obtained previously by spectroscopic methods for type I water, *i.e.*, H-O-H near (100) with the H-H vector nearly parallel to  $c$ . However, no evidence was found in the  $\Delta\rho$  maps for type II water. A peak ascribed to the alkali atoms that centers the six-membered ring

becomes elongated parallel to  $c$  upon heating through  $375^{\circ}\text{C}$ , while the peak ascribed to the oxygen associated with  $\text{H}_2\text{O}$  is absent in the Mg-cordierite at  $775^{\circ}\text{C}$  and in the Fe-cordierite at  $375^{\circ}\text{C}$ . After heating the Mg-cordierite to  $775^{\circ}\text{C}$  the peak reappeared in the  $\Delta\rho$  maps computed from data recorded at  $24^{\circ}\text{C}$ , but it no longer showed an elongation parallel to  $a$  as it did before heating.